Structural Biology and Molecular Biophysics
Microbiology and Infectious Disease

Secreted dengue virus NS1 from infection is predominantly dimeric and in complex with high-density lipoprotein

Reviewed Preprint

Revised by authors after peer review.

About eLife's process

Reviewed preprint version 2
February 20, 2024 (this version)

Reviewed preprint version 1
November 3, 2023

Posted to preprint server
August 1, 2023

Sent for peer review
July 22, 2023

Bing Liang Alvin Chew, An Qi Ngoh, Wint Wint Phoo, Kitti Wing Ki Chan, Zheng Ser, Nikhil K Tulsian, Shiao See Lim, Mei Jie Grace Weng, Satoru Watanabe, Milly M. Choy, Jenny G. Low, Eng Eong Ooi, Christiane Ruedl, Radoslaw M. Sobota, Subhash G. Vasudevan, Dahai Luo

Lee Kong Chian School of Medicine, Nanyang Technological University; EMB 03-07, 59 Nanyang Drive, Singapore 636921 • NTU Institute of Structural Biology, Nanyang Technological University; EMB 06-01, 59 Nanyang Drive, Singapore 636921, Singapore • Program in Emerging Infectious Diseases, Duke-NUS Medical School; 8 College Road, Singapore 169857, Singapore • Functional Proteomics Laboratory, Institute of Molecular and Cell Biology, Agency for Science, Technology and Research (A*STAR); 61 Biopolis Drive, Proteos, Singapore 138673, Singapore • Department of Biological Sciences, National University of Singapore, Singapore • Singapore Centre for Life Sciences, Department of Biochemistry, National University of Singapore, Singapore, Singapore • Department of Infectious Diseases, Singapore General Hospital, Singapore, Singapore • Yong Loo Lin School of Medicine, National University of Singapore, Singapore, Singapore • Saw Swee Hock School of Public Health, National University of Singapore, Singapore, Singapore • School of Biological Sciences, Nanyang Technological University, Singapore, Singapore • Department of Microbiology and Immunology, National University of Singapore; 5 Science Drive 2, Singapore 117545, Singapore • Institute for Glycomics (G26), Griffith University Gold Coast Campus, QLD 4222, Australia

Abstract

Severe dengue infections are characterized by endothelial dysfunction shown to be associated with the secreted nonstructural protein 1 (sNS1), making it an attractive vaccine antigen and biotherapeutic target. To uncover the biologically relevant structure of sNS1, we obtained infection-derived sNS1 (isNS1) from DENV-infected Vero cells through immunoffinity purification instead of recombinant sNS1 (rsNS1) overexpressed in insect or mammalian cell lines. We found that isNS1 appeared as an approximately 250 kDa complex of NS1 and ApoA1 and further determined the cryoEM structures of isNS1 and its complex with a monoclonal antibody/Fab. Indeed, we found that the major species of isNS1 is a complex of the NS1 dimer partially embedded in a High-Density Lipoprotein (HDL) particle. Cross-linking mass spectrometry (XL-MS) studies confirmed that the isNS1 interacts with the major HDL component ApoA1 through interactions that map to the NS1 wing and hydrophobic domains. Furthermore, our studies demonstrated that the sNS1 in sera from DENV-infected mice and a human patient form a similar complex as isNS1. Our results report the molecular architecture of a biological form of sNS1 which may have implications for the molecular pathogenesis of dengue.

Summary

CryoEM structures of secreted dengue virus NS1 protein reveal dimers in complex with high-density lipoprotein.

eLife assessment

This potentially **useful** study aims to advance our understanding of the structure of the native form of a viral toxin secreted from infected cells. While some of the findings confirm previous reports, the new claims in this study are unfortunately only **inadequately** supported by the methods and analyses used. More rigorous approaches are needed to justify the main conclusion that the structure of the viral toxin derived from infected cells in this study is distinct from previously reported structures of recombinantly expressed versions of the toxin.

Introduction

Dengue virus (DENV) is a member of the flavivirus genus and is the cause of significant healthcare problems and economic burden worldwide, partially due to the lack of effective therapeutics and the limited efficacy of licensed vaccines, Dengvaxia® and QDENGA®[1,2]. While the majority of DENV infections are mild or asymptomatic, severe dengue infections, marked by vascular leakage, can be life-threatening and even fatal. The severity of dengue infections has been demonstrated to be correlated to high sera levels of sNS1 in clinical studies[3,4]. The viral nonstructural protein 1 (NS1) is a highly conserved and multifunctional protein that exists as intracellular membrane-associated NS1, a presumed GPI-anchored outer plasma membrane-associated NS1, and secreted NS1 (sNS1) during viral infection[5]. NS1 could interact with a myriad of proteins associated with its immune evasion and virotoxin roles[6]. The interactions of NS1 with viral E protein[7] and the NS4A-2K-NS4B precursor protein[8] have been shown to be important in virus production and replication respectively. Intracellular NS1 found in the ER lumen is an essential part of the membranous viral RNA replication compartment[7]. Upon release from the cells, sNS1 enters the blood circulation where *in vitro* and *in vivo* mouse evidence have demonstrated its ability to induce vascular permeability, a hallmark of severe dengue, either independently[9] or through inducing pro-inflammatory responses[10].

The high-resolution crystal structures of NS1 dimer have been reported for DENV[11], WNV[11], and ZIKV[12,13] which provide a conserved molecular view of flaviviral NS1. Mature NS1 is 352 amino acids long with an apparent molecular mass between 40 – 50 kDa depending on its glycosylation state. NS1 has a three-domain architecture, a hydrophobic β-roll (residues 1-29), an α/β wing (38-151), and a β-ladder (181-352). The connector segments between the wing and β-ladder domains, residues 30-37 and 152-180, form a 3-stranded β-sheet. The dimer has a distinct cross shape with the wings extending from the central β-ladder which has an extended β-sheet that faces the hydrophobic β-roll and a “spaghetti loop” on the opposite hydrophilic outer face that lacks structured elements[11–13]. sNS1 was reported to be a barrel-shaped hexamer with lipid cargo held together by hydrophobic interactions based on biophysical and low-resolution EM analysis[14–16]. Recent cryoEM structures of recombinant sNS1 (rsNS1) from DENV-2 showed mainly tetrameric rsNS1 with only 3% of the population found to be in the hexameric form[17]. While earlier studies by Gutsche et al (2011) found that the lipid profile of DENV-1 infection-derived sNS1 to be similar to high-density lipoprotein (HDL)[15], the same research group now showed that DENV-2 rsNS1 could dock onto HDL with direct visualization using negative stain EM

analysis as reported by Benfrid et al. (2022)[18]. Additionally, sNS1 appears to utilize the scavenger receptor B1, a known receptor for HDL, as the cognate receptor in cultured cells[19]. Since the interactions of sNS1 with the target cells implicated in pathogenesis require the hydrophobic β-roll side to be exposed[11], the mechanism by which the oligomeric sNS1 with its lipid load in the central channel dissociates and associates have been a topic of intense research interest[18,20,21]. However, the native structure of the extracellular NS1 during viral infection remains unclear.

To closely mimic of sNS1 circulating in dengue patients' sera, we obtained infection-derived sNS1 (isNS1) from the culture supernatant of Vero cells infected with either the DENV2 WT (isNS1wt) or T164S mutant (isNS1ts). The T164S mutation in the greasy finger loop between the wing and β-ladder interdomain of NS1 was identified from a DENV2 epidemic in Cuba in 1997, where a correlation with enhanced clinical disease severity was observed[22]. We demonstrated that this single mutation in NS1 could directly cause lethality in mice and increased sNS1 secretion[23], which served as an epidemiologically relevant tool to study the biochemical and structural characteristics of sNS1 in this study.

We determined that the isNS1 is a complex of the NS1 dimer embedded on a single HDL particle composed of ApoA1. By applying integrative structural tools, we report the cryoEM structural model of the purified isNS1:HDL complex at ~8 Å resolution with protein-protein interactions between NS1 and ApoA1 defined by crosslinking mass spectrometry (XL-MS). Furthermore, the Ab56.2 binding site model in the cryoEM model of isNS1:ApoA1 complex was elucidated using hydrogen deuterium exchange mass spectrometry (HDX-MS) as well as NS1 peptide competition ELISA. Interrogation of DENV-infected mouse sera and a human patient suggests that the sNS1:HDL complex exists *in vivo* as a similar complex to isNS1.

Results

Native isNS1 is a complex of NS1 with ApoA1

We purified sNS1 using a monoclonal antibody 56.2 from the supernatant of the infected Vero cell cultures (**Fig. 1a** and Supplementary Fig. 1a-b). Initial negative stain screening of the isNS1wt (Supplementary Fig. 1c) showed some 2D classes of NS1 dimers presumably docked onto a spherical density, mirroring the *in vitro* reconstitution of crsNS1 with HDL complex negative stain microscopy results by Benfrid et al. (2022)[18]. Both immunoaffinity purified isNS1wt (**Fig. 1b** and Supplementary Fig. 2a) and isNS1ts (Supplementary Fig. 2a and 3b) retained a molecular size of ~250 kDa as detected with Coomassie Blue (**Fig. 1b** and Supplementary Fig. 2a) and on a Western blot using Ab56.2 following separation on a Native-PAGE (**Fig. 1b**), as previously reported[23]. The isNS1wt migrated slower than the rsNS1 protein (a gift from Shu et al. 2022[17]), indicating possible conformational or oligomeric differences between the two NS1 species (**Fig. 1b**). On a reducing SDS-PAGE, we identified two major bands of approximately 50 kDa and 25 kDa in isNS1wt, the former corresponding to the single monomeric NS1 band seen in rsNS1 (**Fig. 1c**). Preliminary mass ID identified the 25 kDa protein as bovine apolipoprotein A1 (ApoA1), a major component of HDL in bovine serum-containing culture media, which has a reported molecular weight of 28 kDa[24]. Hence, the two bands were further validated on a Western blot, which confirmed the 50 kDa band as NS1 and the 25 kDa band as ApoA1 respectively (**Fig. 1c**). The same observations were seen in isNS1t (Supplementary Fig. 3).

Next, we elucidated the composition of the prominent 250 kDa band observed in the Native-PAGE by label-free quantification (LFQ) analysis of proteins using liquid chromatography–mass spectrometry (LC-MS). We obtained LC-MS data for the ~250 kDa protein excised from the Native-PAGE separation of the immunoaffinity purified isNS1wt (represented in **Fig. 1b**, purple box as Gel Band 1); an aliquot of the elute fraction from immunoaffinity purification (depicted in **Fig.**

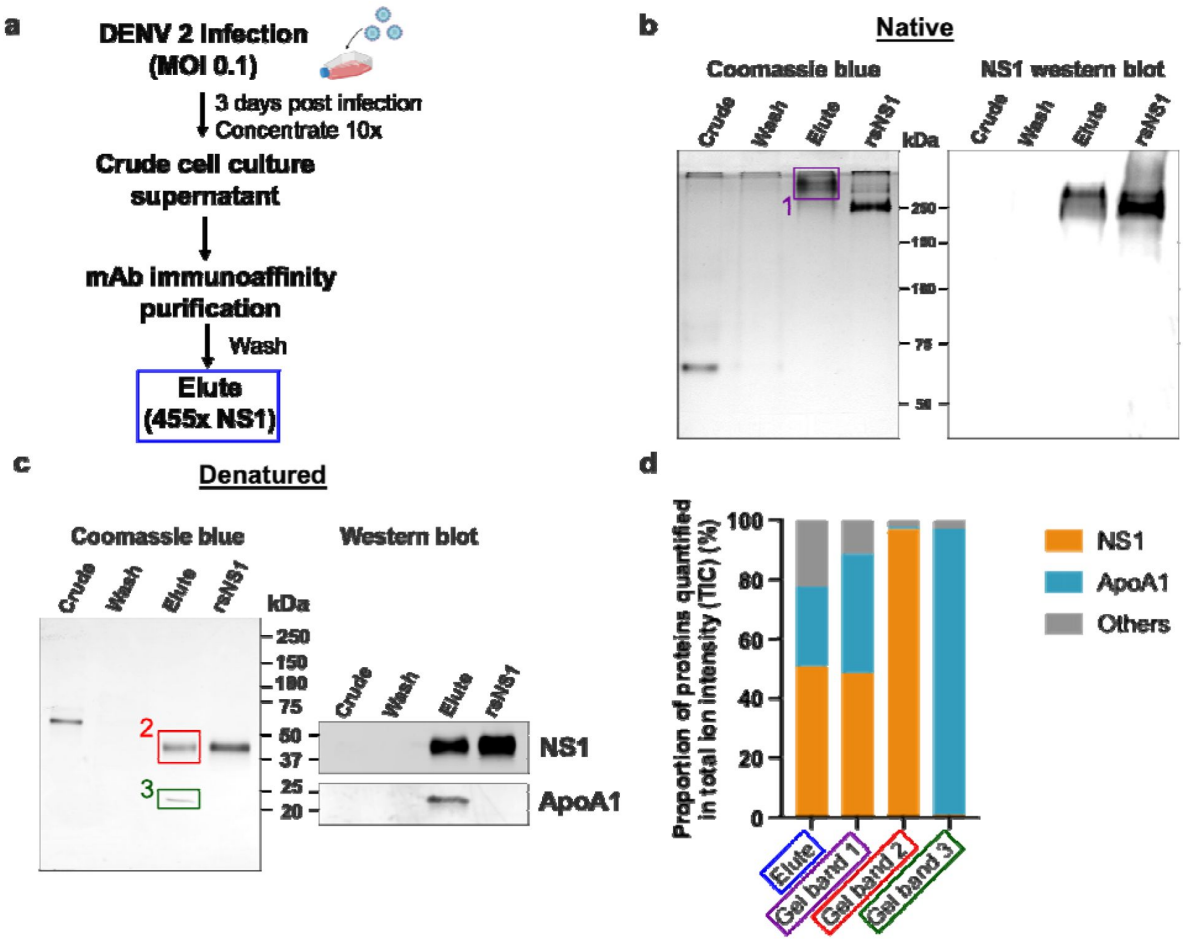

Fig. 1.

Composition of the secreted NS1 from DENV-infected Vero cells.

DENV 2 WT cell culture supernatant was filtered, supplemented with protease inhibitor cocktail and 0.05% sodium azide, concentrated using a 100 kDa MWCO Vivaflow cassette and purified using 56.2 anti-NS1 antibody immunoaffinity chromatography. The eluted isNS1wt was dialysed against PBS, concentrated, and stored at –80°C until further use. **(a)** Schematic of isNS1 purification to illustrate the samples used for gel analyses. % NS1 is measured by the total amount of NS1 (quantified using the anti-NS1 ELISA kit (Bio-rad) as a percentage of total protein (quantified using the Bradford assay) found in each sample. Details of the % enrichment in NS1 along the purification process is as shown in Supplementary Fig. S1 B. **(b)** Coomassie blue detection of proteins from Crude, Wash and Elute immunoaffinity fractions for isNS1wt, with the recombinant sNS1 (rsNS1) obtained from Shu et al (2022)[17] as a positive control, after separation on a 10% Native-PAGE gel (left). The Crude and Elute fractions contain 1 µg of total protein. The Wash fraction contains approximately 100 ng of total protein in maximum well volume of the gel. The same set of samples were also subjected to a western blot detection of NS1 using 56.2 anti-NS1 antibody after separation on a 10% Native-PAGE (right). The Crude and Elute fractions contain 500 ng of total protein. The Wash fraction contains approximately 100 ng of total protein in maximum well volume of the gel. **(c)** Coomassie blue detection of proteins from Crude, Wash and Elute immunoaffinity fractions for isNS1wt and rsNS1[17], after separation on a 4-20% reducing SDS-PAGE gel. The Crude and Elute fractions contain 1 µg of total protein. The Wash fraction contains approximately 100 ng of total protein in maximum well volume of the gel. Similarly, the same set of samples were also subjected to a western blot detection of NS1 and ApoA1 using 56.2 anti-NS1 antibody or ApoA1 antibody (Biorbyt, orb10643) respectively, after separation on a 4-20% reducing SDS-PAGE (right). **(d)** In-gel protein identification of the purified isNS1wt by liquid chromatography mass spectrometry (LC-MS). Proportion of NS1, ApoA1 and other unidentified proteins quantified in total ion intensity, obtained from the following samples: Elute in solution (boxed in blue), 250 kDa gel band (boxed in purple), 50 kDa gel band (boxed in red) and 25 kDa gel band (green). The boxed gel bands are from representative gels showing the different protein species found while the actual gel bands used for protein identification by LC-MS are as shown in Supplementary Fig. 2a-b.

1a blue box and referred to as "Elute") and the 50 kDa and 25 kDa bands excised after separation of the elute fraction on a reducing SDS-PAGE (**Fig. 1c**, represented by red and green boxed labelled as Gel Band 2 and 3 respectively) as positive controls. The raw data for the ion intensities of the samples tested are as detailed in Supplementary File 1. We found that the combined LFQ intensity of NS1 and ApoA1 accounted for more than 77.6% and 88.6% of the total ion intensity count (TIC) detected from the elute fraction (**Fig. 1a**, blue box) and the 250 kDa band (**Fig. 1b**, the purple box labelled '1') respectively, indicating that NS1 and ApoA1 were the major proteins in the elute fraction and the ~250 kDa band from immunoaffinity purified isNS1wt (**Fig. 1d**). Accordingly, as depicted in **Fig. 1d**, NS1 accounted for 96.85% of the TIC for the 50 kDa band (**Fig. 1c**, red box '2'), while the intensity of ApoA1 accounted for 96.23% of the TIC for the 25 kDa band (**Fig. 1c**, green box '3'). Similar LFQ analysis of LC-MS data for the purified isNS1ts mutant showed that NS1 and ApoA1 were the major components (Supplementary Fig. 2) of the respective Elute and ~250 kDa gel band on Native-PAGE (Supplementary Fig. 2a; 3a, purple box). The corresponding 50 kDa and 25 kDa gel bands on the reducing SDS-PAGE (Supplementary Fig. 2b, 3b) identified as NS1 and ApoA1 by immunoblotting with the respective antibodies (Supplementary Fig. 3b), were further confirmed by LC-MS as NS1 and ApoA1 (Supplementary Fig. 2c, 3c, Supplementary file 1). Taken together, the results from the Native PAGE and LFQ by LC-MS strongly indicated that the isNS1 purified from the supernatant of infected cells *in vitro* is an approximately 250 kDa complex of NS1 and ApoA1.

CryoEM structure of isNS1

To gain insights into the molecular organization of this native isNS1, we determined the cryoEM structure of isNS1 (Supplementary Table 1 and Supplementary Fig. 4-7). The 2D classes of isNS1ts are observed to be heterogenous spheres with some internal features, some of which resembling the cross-shaped NS1 protruding from the sphere (Supplementary Fig. 4b). However, the 3D reconstruction of isNS1ts alone was observed to have no discernible features beyond a spherical-like density with varying dimensions averaging around 106 Å by 77 Å (Supplementary Fig. 4b-c). To obtain higher resolution structural information on the complex, we collected data for the ternary complexes of the isNS1wt:Ab56.2 isNS1wt:Fab56.2 (**Fig. 2a** and Supplementary Fig. 5-6). The use of antibodies as fiduciary markers is a well-proven approach for solving the structures of small proteins[25,26]. Overall, both samples resulted in similarly distinguishable 2D class averages (**Fig. 2b-c**) which show asymmetrical binding of one unit of Fab56.2 to the dimeric cross-shaped sNS1 associated with a lower-density sphere, presumably HDL.

In the isNS1wt:Fab56.2 ternary complex dataset, we further observed two apparent but rare sub-classes of free sNS1wt dimer bound to two units of Fab56.2 representing 3.5% of the total population of picked particles (**Fig. 2c**, red dashed boxes). While the cryoEM map reconstructions remain limited at low resolutions (Supplementary Fig. 5-6), they could be fitted with the NS1 dimer and Fab56.2 models (**Fig. 2d**) predicted separately using AlphaFold2[27,28], with a correlation value of 0.75 to the fitted regions using a simulated 5 Å map from the NS1 dimer and Fab models. The AlphaFold2 predicted model of the NS1 dimer was used despite the availability of the crystallographic dimer model (PBS ID: 6WER)[29] given their high similarity (RMSD: 0.67) and that the latter had a few unmodelled residues (aa 118-128). The map-model fitting showed that the epitope sites were at the tip of the C-terminal β-ladder region. The approximate dimensions of the spherical HDL could also be measured at 82 Å by 65 Å (Supplementary Fig. 5-6) which aligned with existing reports of spherical HDL being measured at 70-120 Å in diameter with predominantly homodimeric ApoA1 arranged as an anti-parallel double-belt stabilized by intermolecular salt bridges[30,31]. We predicted a model of an antiparallel dimer of ApoA1 using AlphaFold2[27,28] without the first 58 residues of ApoA1 as the N-terminal domain is highly flexible[30]. The model has a cross-sectional distance of approximately 78 Å and fits into the spherical density in the cryoEM map. The NS1 dimer appears semi-embedded on the HDL particle through its hydrophobic surface, with a conformation that

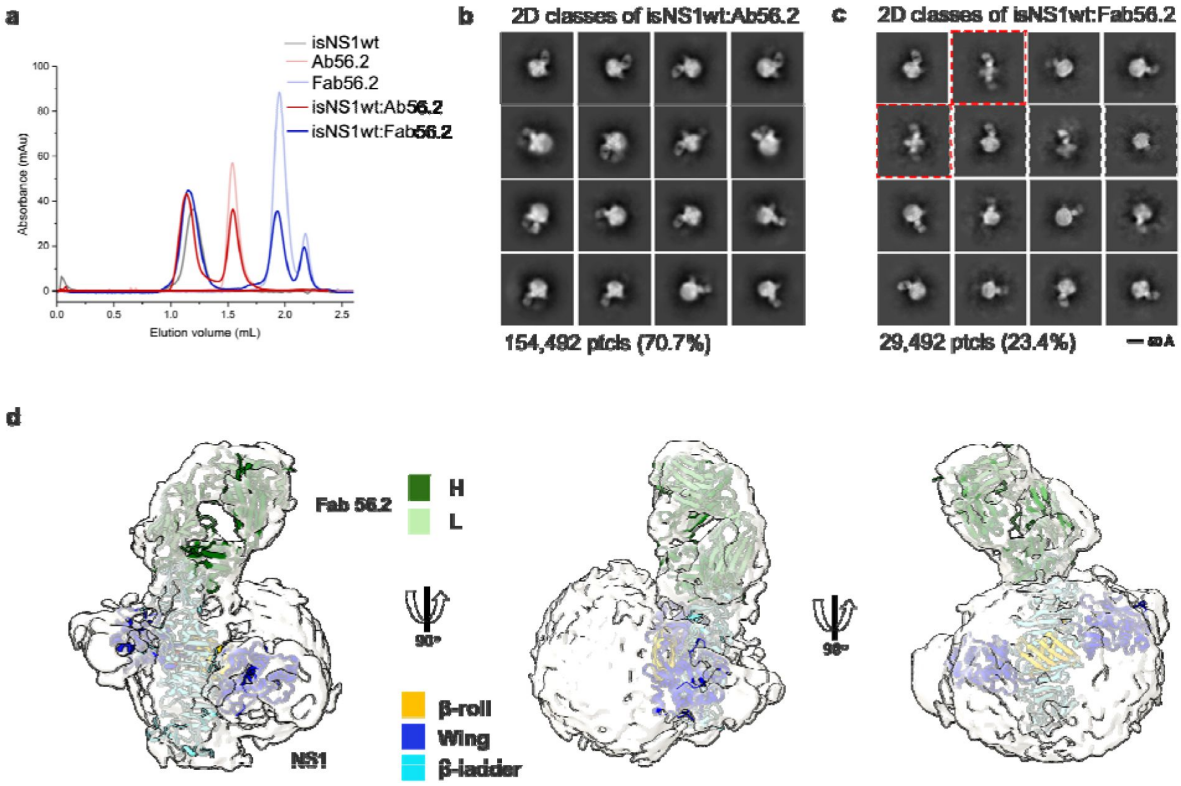

Fig. 2.

CryoEM analysis of secreted NS1 in complex with antibody Ab56.2.

(a) Size exclusion chromatography was run on a Superdex 200 increase 3.2/300 GL column connected to the ÄKTA purifier with a flow rate of 0.075 mL/min in PBS (pH 7.4) for purified isNS1wt (gray), Ab56.2 (faded red), Fab56.2 (faded blue), isNS1wt:Ab56.2 (red) and isNS1wt:Fab56.2 (blue). A slight leftward shift in elution volume was observed for isNS1wt upon complexing with Ab56.2 and Fab56.2. 2D class averages of **(b)** isNS1wt:Ab56.2 and **(c)** isNS1wt:Fab56.2 showing representative sub-class of the Fab56.2:isNS1:HDL particles with black scale bar, 50 Å. The corresponding number of particles and percentages are listed below the respective boxes. Red dashed line boxes highlight two rare views consisting of 1033 particles (3.5%) only seen in isNS1wt:Fab56.2 sample. **(d)** Model of isNS1wt:Fab56.2 predicted structures rigid body fitted in the CryoEM map of Fab56.2:isNS1:HDL (grey, contoured at 0.14) with correlation value of 0.75 to the fitted regions (map simulated from atoms at 5 Å). isNS1wt is coloured by its three domains, namely the β-roll (orange), wing (blue), and β-ladder (cyan). Fab56.2 is coloured by it heavy chain (dark green) and light chain (light green).

exposed only one end of the β-ladder domain to which Ab56.2 and Fab56.2 bind. Overall, the cryoEM model indicated that the purified ~250 kDa isNS1 is a complex of a NS1 dimer and HDL, consistent with the gel and LFQ analysis of LC-MS data presented above.

Similarly, we determined the structures of the ternary complex of isNS1ts mutant with Fab56.2 (**Fig. 3a**). Interestingly, 2D class averages of isNS1ts:Fab56.2 dataset showed a significant sub-population of a free NS1ts dimer bound to two units of Fab56.2 (53.7%), in addition to the HDL spheres (23.6%) and isNS1ts dimer:HDL:Fab56.2 (22.7%) classes (**Fig. 3b** and Supplementary Fig. 7). The predicted structure of the isNS1ts dimer bound to Fab56.2 could be fitted with an overall correlation value of 0.5 using map simulated from atoms at 5 Å (**Fig. 3c**). Achieving atomic resolution to map the Fab binding interface with the NS1 β-ladder domain remains a challenge due to the preferred orientation (Supplementary Fig. 7). A comparison of the cryoEM density maps of free isNS1ts dimer:Fab56.2 (**Fig. 3D**, grey) and isNS1ts dimer:HDL:Fab56.2 ternary complex (**Fig. 3d**, yellow) fitted with a correlation value of 0.71 based on the NS1 map region, revealed a pose difference of the Fab56.2 between the free isNS1ts dimer and the HDL-bound isNS1ts dimer (**Fig. 3d**, inset). Further comparison of the density maps of the isNS1 dimer:HDL population in the Fab56.2 ternary complexes of isNS1wt (**Fig. 3e**, purple) and isNS1ts (**Fig. 3e**, yellow) revealed conformational similarities of the isNS1 dimer:HDL complex.

XL-MS maps the inter- and intra-molecular architecture of the isNS1

Next to refine our understanding of the NS1 dimer:HDL complex of the isNS1 indicated by the LFQ of LC-MS (**Fig. 1d** and Supplementary Fig. 3d) and cryoEM results (**Fig. 2d** and **3d**), we probed the interactions between NS1 and ApoA1 - the major protein moiety of HDL - using crosslinking mass spectrometry (XL-MS)[32] on the immunoaffinity purification eluate fraction (**Fig. 4a**, Supplementary Fig. 8a-b). We identified 28 NS1:NS1 and 29 ApoA1:ApoA1 intramolecular crosslinks, as well as 25 NS1:ApoA1 intermolecular crosslinks for isNS1wt (**Fig. 4b**; Supplementary File 2a-b). As depicted in **Fig. 4b-c**, the NS1 residues that are involved in both intra- and inter-molecular crosslinks were located mainly on the β-roll and wing domains, with ~34% of the NS1:ApoA1 crosslinks being located on the β-roll domain. The NS1:NS1 intramolecular crosslink pairs were further validated on the predicted NS1 dimer model by implementing a 30 Å cut-off distance for the Cα atoms of crosslinked residues, a criterion that was met by 85% of the NS1:NS1 intramolecular crosslinks (24 out of 28; **Fig. 4d**). The NS1:ApoA1 intermolecular crosslinks for the immunoaffinity purified isNS1wt were found to be located between the β-roll and wing domains of NS1 and the helices 3, 4, 8 and 10 of ApoA1 (**Fig. 4b, d**). Applying the same cut-off value of <30 Å distance between the Cα atoms of the NS1:ApoA1intermolecular crosslinked residues and validating it on the cryoEM model of isNS1wt in this study (**Fig. 4d-e**) satisfied 76% of the crosslinks (19 out of 25 intermolecular crosslinks between NS1 dimer and ApoA1). In the case of ApoA1:ApoA1 intramolecular crosslinks, the <30 Å distance between their Cα atoms cut-off satisfied 62% of the crosslinks (18 out of 29 ApoA1:ApoA1 intramolecular crosslinks). The higher number of violated crosslinks in ApoA1:ApoA1 compared to those in NS1:NS1 could be due to the flexible and dynamic nature of ApoA1 dimers which may prevent it from assuming a fixed relative position among the ApoA1 dimer population in the HDL. Overall, the XL-MS data and structural validation agreed with the cryo-EM model of isNS1 being a complex of the NS1 dimer embedded on a HDL particle composed of an ApoA1 dimer (**Fig. 4d-e**).

Additionally, the XL-MS mapping of isNS1ts mutant (Supplementary Fig. 8c-d) followed by rigid-body fitting into the corresponding cryoEM map (Supplementary Fig. 8e) revealed a similar crosslink pattern to isNS1wt, except that there were fewer crosslink sites (Supplementary Fig. 8f, Supplementary File. 2a). This indicated that isNS1ts dimer may have a weaker affinity to HDL in

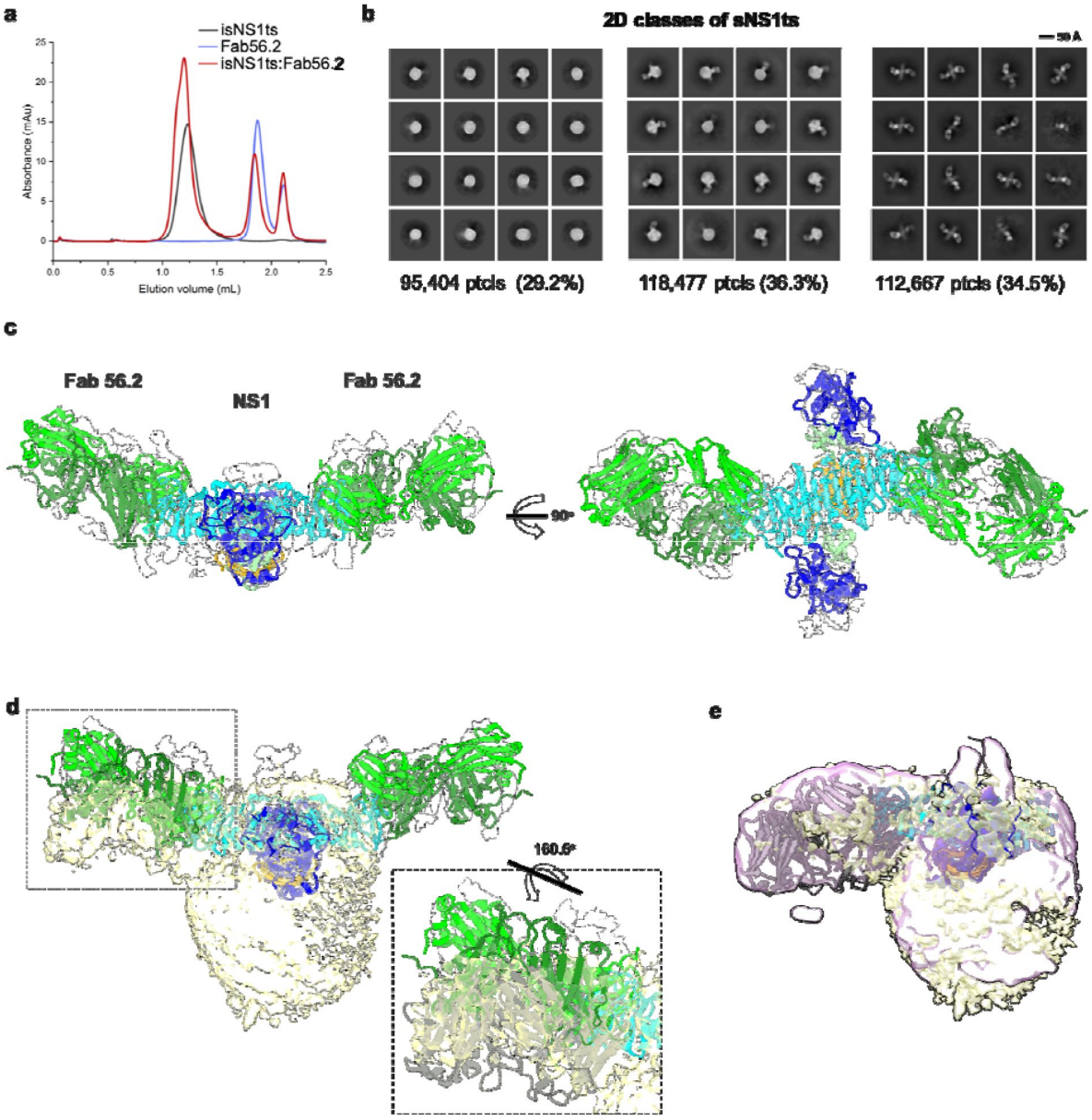

Fig. 3.

Secreted NS1 forms free dimers in complex with antibody Ab56.2.

(a) Size exclusion chromatography was run on a Superdex 200 increase 3.2/300 GL column connected to th AKTA purifier with a flow rate of 0.075mL/min in PBS (pH 7.4) for purified isNS1ts (gray), Fab56.2 (faded blue) and isNS1ts:Fab56.2 (red). A similar leftward shift in elution volume wa also observed for isNS1ts upon complexing with Fab56.2. **(b)** 2D class averages of isNS1ts:Fab56.2 dataset with 326,548 particles picked and separated into 3 distinct populations, HDL spheres, Fab56.2:isNS1:HDL, and free isNS1:Fab56.2. Black scale bar, 50 Å, as indicated. The corresponding number of particles and percentages are listed below the respective boxes. **(c)** Model of isNS1ts dimer and Fab56.2 predicted structures rigid body fitted in the isNS1ts:Fab56.2 density map (grey, contoured at 0.14) with correlation value of 0.53 (overall, map simulated from atoms at 5 Å). isNS1ts is coloured by its three domains, namely the β-roll (orange), wing (blue), and β-ladder (cyan). Fab56.2 is coloured by its heavy chain (dark green) and light chain (light green). **(d)** Density map fitting between isNS1ts:Fab56.2 (grey, contoured at 0.14) to Fab56.2:NS1ts:HDL (yellow, contoured at 0.1) with correlation value of 0.53 (overall) and 0.7137 (on D2NS1 map region only). Inset shows the difference in the pose of Fab from the free NS1 form to the HDL-bound form. (e) Density map fitting between Fab56.2:isNS1wt:HDL (purple, contoured at 0.05) to Fab56.2:NS1ts:HDL (yellow) with correlation value of 0.72 (overall).

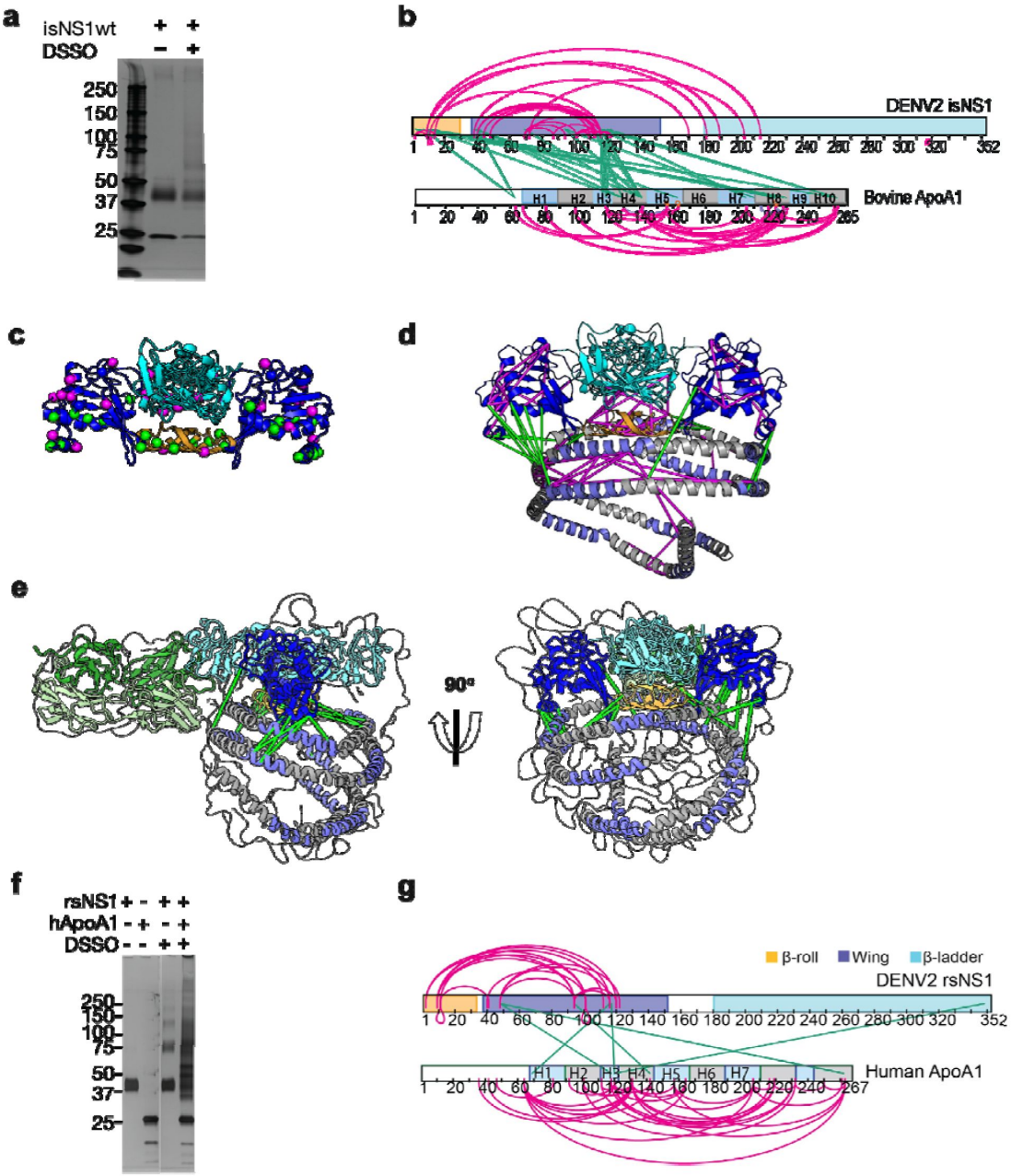

Fig. 4.

Interaction sites of NS1:ApoA1 complex identification by crosslinking mas spectrometry.

(a) SDS-PAGE analysis of isNS1wt with or without the addition of DSSO crosslinker. **(b)** The identified crosslinks are visualised on the NS1 and bovine ApoA1 constructs. The intramolecular (NS1:NS1 and ApoA1:ApoA1) crosslinks are in magenta. Th intermolecular NS1:ApoA1 crosslinks are in green. **(c)** The isNS1 residues that are involved in NS1:NS1 interactions are visualised on the NS1 dimer model. The NS1 cartoon model i coloured by its three domains, namely the β-roll (orange), wing (blue), and β-ladder (cyan) with the intramolecular (magenta) and intermolecular (green) crosslinking sites depicted as spheres. **(d)** The overall model interpretation of NS1:ApoA1 complex within the crosslinker theoretical distance cut-off at =< 30 Å as depicted. ApoA1 dimer cartoon model with its conserved helices as labelled coloured in intervals of grey and light purple. **(e)** The NS1:ApoA1 dimer model with validated crosslinks were fitted into the cryoEM envelope. **(f)** SDS-PAGE analysis of crosslinked rsNS1 alone or with human HDL **(Lanes 3-5)**. Non-crosslinked rsNS1 and Human HDL are the control **(Lanes 1-2)**. The crosslinked rsNS1 can be seen in higher oligomers **(Lane 3)**. **(g)** Identified crosslinks are mapped on the NS1 and ApoA1 constructs, coloured as per panel B.

comparison to the isNS1wt dimer. This finding is consistent with the cryoEM data for isNS1ts where we found that free isNS1ts dimers bound to Fab56.2 formed a significant sub-population (34.5%) of the total picked particles (**Fig. 3b**, Supplementary Fig. 7b).

Given the reported structures of hexameric and tetrameric rsNS1 from mammalian expression systems, insect cells[11,15,16,29] and Expi293 HEK cells[17], we further examined whether rsNS1 oligomerizes in the presence of exogenously added human HDL, using XL-MS. The crosslinked rsNS1 alone appeared as higher oligomer bands of dimers, tetramers, and hexamers on the SDS-PAGE analysis (**Fig. 4f**, lane 3) which differed from the crosslinked isNS1 (**Fig. 4f**, lane 3). Interestingly, the addition of human HDL and crosslinker resulted in a smearing band ranging from 30-150 kDa with the loss of the well-defined monomeric rsNS1 band (**Fig. 4f**, lane 4). In the crosslinked rsNS1 in the absence of HDL, we identified 17 NS1:NS1 intramolecular crosslinks at the β-roll and wing domains (**Fig. 4f-g**, Supplementary File 3a-b). In the presence of human HDL, we identified 30 ApoA1:ApoA1, 4 NS1:NS1, and 6 NS1:ApoA1 crosslinks (Supplementary File 3a-b). Most crosslinks identified are ApoA1:ApoA1 intramolecular crosslinks in the rsNS1:ApoA1 samples (**Fig. 4g**). Only 1 out of 6 rsNS1:ApoA1 intermolecular crosslinks was within the 30 Å cutoff distance when mapped to the NS1:ApoA1 cryoEM model (**Fig. 4e**). This was in stark contrast with the isNS1 samples where the number of crosslinks between ApoA1:ApoA1, sNS1:sNS1, and sNS1:ApoA1 was similar (**Fig. 4b**). Overall, this suggests that rsNS1 may form oligomers of dimers but not a complex with HDL under the tested conditions.

Ab56.2 binds at the C-terminal β-ladder region of NS1

The cryoEM map for isNS1wt:Fab56.2 reliably placed the epitope site of Ab/Fab56.2 at the C-terminal b-ladder region, although the precise identification of the epitope site was hindered by the limited resolution of the cryoEM maps (**Fig. 2**-**3**, Supplementary Fig. 4-7). Attempts to improve the resolution were challenging so we resorted to using a truncated form of recombinant secreted NS1 consisting of only the C-terminal region (rsNS1c; residues 172-352) to determine Ab56.2 epitope. The rsNS1c fragment of residues 172-352 was previously used for structural studies of dengue[33,34] and other flaviviruses, West Nile virus[33], Zika virus[34,35], and Japanese encephalitis virus[36]. The epitope region of Ab56.2 was first confirmed by overlapping 15-mer NS1 peptide competition ELISA for Ab56.2 binding (Supplementary Fig. 9a, Supplementary Table 2). The greatest competition was observed at the NS1 peptide spanning residues 316-330 out of 301-340 which showed a decrease in OD450 absorbance (Supplementary Fig. 9b). We further applied the hydrogen-deuterium exchange mass spectrometry (HDX-MS) to monitor the conformational dynamics between Fab56.2 and NS1c to obtain higher peptide-level resolution for the binding interface. Comparative HDX results revealed global scale protection against deuterium exchange of NS1c in the presence of Fab56.2 (**Fig. 5a**, Supplementary Fig. 10a), indicative of reduced conformational dynamics. Large-scale differences in deuterium exchange were primarily observed across peptides spanning the dimer interface (residues 174-186) and at the tip of the C-terminal β-ladder (residues 286-347) of NS1c (**Fig. 5b**). Multiple overlapping peptides, spanning residues 286-347 (**Fig. 5b**), showed protection against deuterium exchange even at the longer labeling times (100 min) in NS1c:Fab56.2 complex (Supplementary Fig. 10a, Supplementary File 4). These results suggest that Fab56.2 bound stably with NS1c. Coupled with the observation that the most significant change in the differential plot was at residues 300-310 (**Fig. 5a**), these results collectively indicate that NS1c binds stably to Fab56.2 at the primary epitope site of residues 300-310.

Comparative HDX results of NS1c-bound and free Fab56.2 revealed protection against deuterium exchange of all three complementarity-determining regions (CDR) of the heavy chain (**Fig. 5c**, Supplementary Fig. 10b) and CDRL2 of the light chain (**Fig. 5d**, Supplementary Fig. 10c). Upon binding to NS1c, peptides spanning CDRH3 (residues 89-116) showed the largest magnitude decrease in deuterium exchange at all labeling time points, while CDRH2 showed minor significant differences. In addition, only the CDRL2 loop (residues 49-56) of the light chain of Fab56.2 showed significantly decreased deuterium exchange. Mapping of the deuterium exchange profiles of

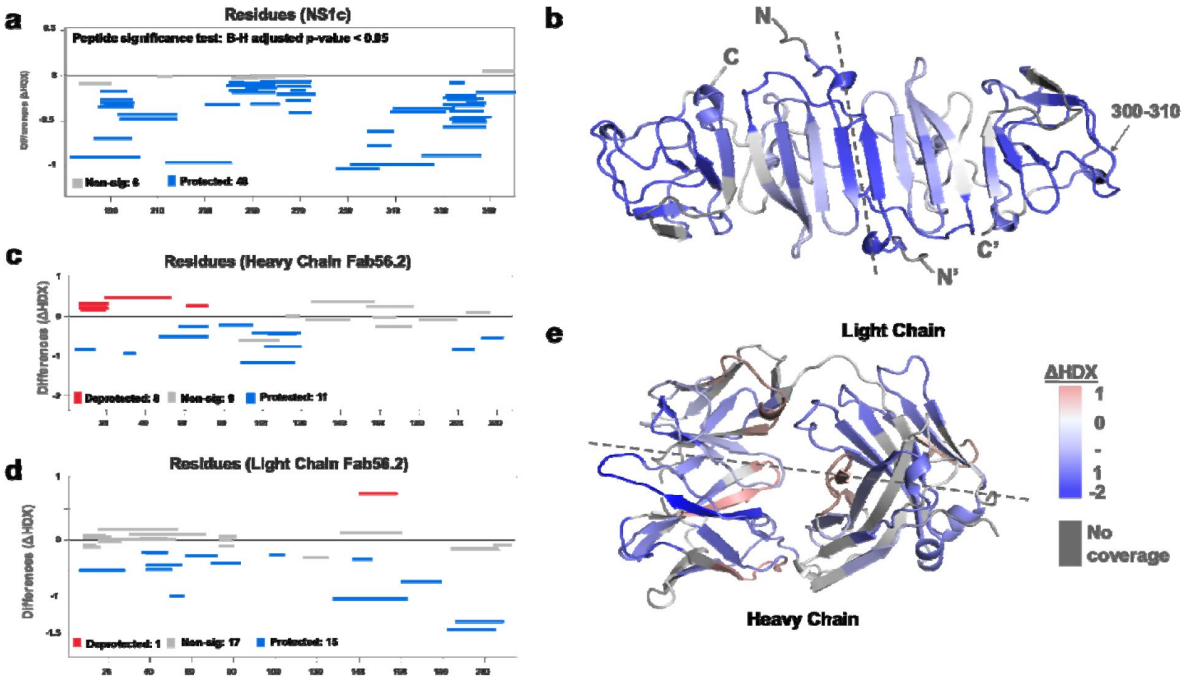

Fig. 5.

Interaction interface of rsNS1c-Fab562 complex characterized by HDX-MS.

(a) Woods differential plot showing the differences in deuterium exchange (y-axis) between Fab562-bound and free NS1c protein across various residues (x-axis) at 10 min labeling timepoint. Negative differences indicate protection against deuterium exchange across NS1c peptides in the presence of Fab562, as compared to free NS1c. A p-value <0.05 is considered a significance threshold, which identified 6 non-significant peptides (grey lines) and 48 protected peptides (blue lines). **(b)** Cartoon representation of NS1c dimer model showing differences in deuterium exchange at 10 min labeling as indicated in key. Dashed line distinguishes the two monomers in the dimer. Peptide spanning residues 300-310 showing the highest protection are indicated. **(c, d)** Woods differential plot comparing the differences in deuterium exchange of Fab562 in the presence and absence of NS1c for various peptides of **(c)** heavy chain, and **(d)** light chain. A p-value <0.05 is considered as significance threshold, which identified deprotected (red lines), non-significant, and protected peptides as indicated. **(e)** Cartoon representation of Fab562 model showing deuterium exchange differences at 10 min mapped for Fab562-NS1c complex, as per key. Plots were generated using Deuteros 2.0, while cartoon structures were generated using PyMoL.

heavy and light chains onto a model of Fab56.2 (**Fig. 5e**) revealed that CDRH1-3 and CDRL2 loops were spatially co-localized to form the paratope site to bind NS1c, with the heavy chain being the primary anchor. Collectively, these results indicated that residue 300-310 of NS1 act as the primary epitope site to bind Fab56.2 and Fab56.2 binds stably with NS1c.

Circulating NS1 is in the form of NS1:HDL complex

Lastly, we sought to provide *in vivo* evidence of NS1 and ApoA1 interaction using sera samples from DENV-infected mice and a human patient. Since we previously showed that DENV2 T164S mutant virus led to more severe disease in the AG129 mouse model[23], we used the same infection model to obtain pooled mice serum for immunoaffinity purification of sNS1ts as described in Supplementary Fig. 1. The mouse sera immunoaffinity purified sNS1ts was detected at ~250 kDa by both anti-ApoA1 and anti-NS1 antibodies in a Western blot analysis following separation on a Native PAGE (**Fig. 6a**), supporting our mass spectrometry finding that ApoA1 is part of the ~250 kDa isNS1 protein complex purified from infected Vero cells (**Fig. 1d**). We next examined if the isNS1:HDL complex can be detected in dengue patients using serum samples obtained from the CELADEN clinical trial[37]. A primary infection sample with high levels of sNS1 (>15 μg/ml) detected by commercial Platelia™ NS1 ELISA was selected for this purpose to avoid the confounding factor of the presence of anti-NS1 Abs in the secondary infected patients and to pull-down sufficient sNS1 from the patient serum. The patient serum was first subjected to a pre-clearing step using Protein AG resin to reduce the abundance of human IgGs that may interfere with the downstream analysis. We then subjected the pre-cleared patient serum to immunoprecipitation using commercial polyclonal anti-ApoA1 antibodies to pull down and detect ApoA1 and possibly sNS1. Increasing the anti-ApoA1 antibody from 10 to 50 μg coupled onto Protein AG resin for pull-down resulted in a corresponding increase in the sNS1 amount detected by ELISA (**Fig. 6b**), suggesting a specific association between sNS1 and ApoA1. Collectively, despite the limited amount of sNS1 in sera samples from DENV-infected mice or humans, our data points to the association of ApoA1 with sNS1 *in vivo*.

Discussion

In this study, by integrating biochemical and biophysical approaches including immunoaffinity purification, cryoEM, XL-MS and HDX-MS, we have successfully purified and characterised a native population of isNS1. We determined the cryo-EM structure of a natively secreted NS1 from DENV2-infected cells as a ternary complex of NS1 dimer embedded on a single HDL particle. Our in-solution cross-linking mass spectrometry (XL-MS) analysis captured interaction within a cut-off distance of 30 Å imposed by the linker-spacer between the β-roll and wing domains of NS1 and helices 3, 5, 8, and 10 of (bovine) ApoA1 – the main protein moiety of HDL. More importantly, we were able to detect NS1:HDL complexes *in vivo* in both the sera of DENV2-infected mice and in the serum of a DENV1-infected patient, highlighting the biological relevance of the NS1:HDL complexes in dengue infection.

Benfrid et al. (2022) recently reconstituted complexes of rsNS1 dimers bound to the surface of a spheroid human HDL particle *in vitro* at 1:1 to 3:1 ratio when up to 400 μg/mL of rsNS1 were used[18]. Similarly, in our studies with infection-derived sNS1 (isNS1), we observed up to two NS1 dimers docked onto an HDL particle (**Fig. 2**-**3**, Supplementary Fig. 1c, 4-7). It is noteworthy that the concentration of isNS1:HDL in our study (~30 μg/mL) is closer to the maximum clinically reported concentration of sNS1 in the sera of DENV patients (50 μg/mL)[3,38,39]. Therefore, the ratio of sNS1 to HDL varies depending on the concentration of the proteins used for complex formation. Furthermore, the observation that NS1 interacts with HDL regardless of the source of mammalian ApoA1 is unsurprising, given the high sequence similarity of bovine and mouse HDL to human HDL of approximately 79% and 65% respectively (Supplementary Fig. 11) and that the structure of ApoA1 is highly conserved [40].

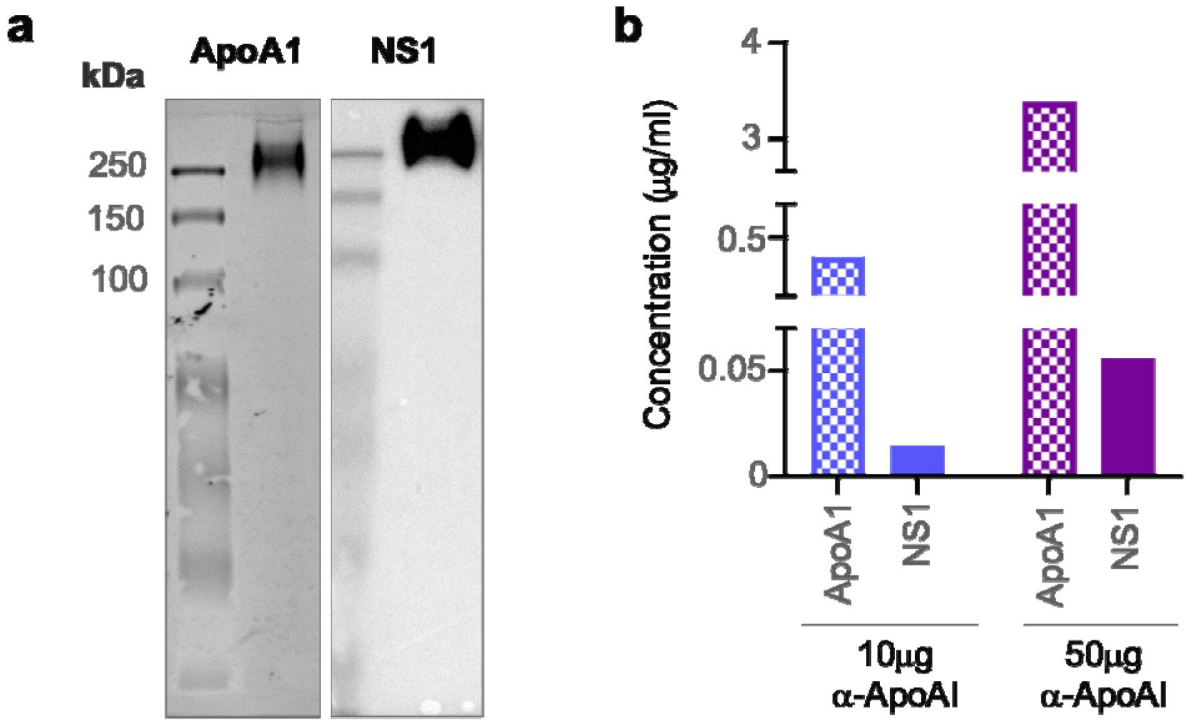

Fig. 6.

sNS1 associates with ApoA1 in DENV infected mouse and human serum.

(a) AG129 mice (n = 10) were infected with DENV2 NS1 T164S mutant virus and the pooled infected sera collected on day 4 post-infection was subjected to NS1 immunoaffinity purification using anti-NS1 56.2 coupled resin as in Supplementary Fig. 1. 2 mg of the purified eluate was then subjected to Western blot analysis after separation and transfer from Native PAGE for detection of ApoA1 and NS1. ApoA1 was detected using the mouse monoclonal anti-ApoA1 clone 513 (Invitrogen, MIA1404) **(left panel)** and the oligomeric NS1 was detected using anti-NS1 56.2 IgG clone **(right panel)**. **(b)** Protein AG resin (Pierce) pre-cleared DENV1 infected patient serum (n = 1) from the CELADEN trial[37] was immunoprecipitated with 10 or 50 mg of rabbit polyclonal anti-ApoA1 antibody (Biorbyt, orb10643) to detect association between ApoA1 and NS1 by ELISA. The amount of ApoA1 and NS1 in the immunoprecipitated sample was determined by human ApoA1 (Abcam, ab189576) and Platelia™ NS1 Ag (Bio-Rad) ELISAs.

Acknowledging the limitation of our study that we used only one antibody (56.2) for our immunoaffinity purification, our key take-home message in terms of structure is that our data does not support the widely-held view that sNS1 is composed of a trimer of NS1 dimers with a ~28 Å wide central channel filled with lipid as established in several seminal publications[14–16]. In fact, our data confirms the observations reported in Benfrid et al.[18] and in the rare instances where trimer of dimers have been experimentally shown by cryoEM of rNS1 structures[17], only a single lipid molecule can be accommodated in the narrow central channel and unlikely to be reflective of sNS1 circulating in serum. We argue that the amount of lipid associated with infection derived sNS1[15,23] is consistent with NS1 dimer(s) associated with HDL. The interaction with HDL requires an exposed hydrophobic face of NS1 which is incompatible to the hexamer model of sNS1. Indeed, it is agreeable that the oligomeric state of NS1 is dynamic which may vary depending on the context and environment. This point requires further independent studies.

Our previous functional studies comparing isNS1wt with isNS1ts (T164S) showed that incubating immunoaffinity-purified sNS1 with human PBMCs from 3 independent human donors triggered the production of proinflammatory cytokines IL6 and TNFa in a concentration dependent manner and that it was more pronounced with the mutant than the WT[23]. Furthermore, we have provisional transendothelial electrical resistance (TEER) assay data with isNS1 proteins used in the structural studies with human umbilical vascular endothelial cells (hUVEC) which show that acid-eluted isNS1 proteins in this study induces endothelial hyperpermeability as shown in previous studies[41]. The presence of a significant population of free isNS1ts dimers in complex with Fab56.2 and fewer crosslinks identified between isNS1ts and ApoA1 point towards the possibility that isNS1ts is more dynamic in its association with host proteins than isNS1wt. The disease severity and increased complement protein expression in AG129 mice liver infected with NS1T164S carrying virus compared with WT that was observed in our previous study [23] can be ascribed to weakly bound mutant NS1 with fast on/off rate with HDL being transported to the liver where specific receptors bind to free sNS1 and interact with effector proteins such as complement to drive inflammation and associated pathology. This notion also requires further validation with other mutations that can impact sNS1 – HDL interaction.

Overall, our work provided a refined understanding of the native structure of sNS1 in DENV pathogenesis. The functional role of HDL-bound NS1 protein in disease is now a topic of contention but one that will be resolved by more data obtained with infection-derived sNS1 by scientists in the field. Contrary to the known protective roles of HDL such as against endotoxic shock caused by lipopolysaccharides[42–44], Benfrid et al. (2022) showed that sNS1:HDL complex triggers proinflammatory signals when tested with primary human macrophages[18]. The presence of sNS1:HDL complexes as a predominant population of sNS1 in our *in vitro* infection model corroborates with a previous report of an interaction between insect-derived recombinant NS1 and the classical HDL/ApoA1-binding receptor known as SR-BI[19], which is primarily expressed on hepatocytes[45]. This interaction in hepatocytes have been suggested to trigger endocytosis of sNS1 and subsequent downstream effects including vascular permeability, which is a characteristic feature of severe dengue[19,46,47]. Internalisation of sNS1 is critical for increased virus production in hepatocytes[46] and NS1-mediated permeability in endothelial cells[47]. Furthermore, NS1:HDL complexes have been shown to induce the production of pro-inflammatory cytokines in macrophages and their presence has been detected in the sera of hospitalised DENV patients[18]. Yet, this hypothesis is confounded by other reports. While rsNS1 has been shown to trigger a TLR4-mediated release of proinflammatory cytokines to induce vascular leakage[48,49], Coelho et al. (2021) further showed that lipid-free recombinant ApoA1 neutralizes the proinflammatory effects caused by insect-derived recombinant intracellular NS1[49]. Furthermore, exogenous administration of purified HEK-293 derived NS1 failed to worsen *in vivo* vascular leakage in sublethally infected mice[50]. This underscores the need for physiologically relevant studies to reconcile these discrepancies and gain a comprehensive understanding of the role of NS1-HDL complex in DENV pathogenesis.

In conclusion, despite the study limitations that our isNS1wt and isNS1ts were immunoaffinity purified with one specific monoclonal antibody (Ab56.2), our structural model, obtained by CryoEM and verified by XL-MS, of infection-derived sNS1 shows a NS1 dimer embedded on a single HDL particle composed of ApoA1 dimer. Future investigation of this work using infected mouse sera from other DENV strains and different flaviviruses would inform the structural and functional relevance of the HDL-bound NS1 protein complex amongst flaviviral NS1 as well as provide a basis for the development of NS1-directed therapeutics.

Acknowledgements

We thank the scientific facility support from NTU Institute of Structural Biology and Protein Product Platform. The authors acknowledge the Cryo-Electron Microscopy Facility at Center for Bioimaging Science, Department of Biological Science, National University of Singapore the scientific and technical assistance. Recombinant DENV2 NS1 protein is a generous gift from Dr Shu Bo and Professor Lok Shee Mei. We thank members of the DL and SV labs for their support.

Funding

This research is supported by the Singapore Ministry of Education under its Singapore Ministry of Education Academic Research Fund Tier 2 (T2EP30220-0020) to DL and National Medical Research Council of Singapore (MOH-OFIRG18may-0006; MOH-OFIRG20nov-0002) to SV, A*STAR core funding and Singapore National Research Foundation under its NRF-SIS “SingMass” scheme to R.M.S, Career Development Award 2021 (A*STAR BMRC) to W.W.P., Career Development Fund 2021 (A*STAR BMRC) to S.Z., and LKCMedicine Dean’s Postdoctoral Fellowship to C.B.L.A.

Author contributions

Conceptualization: SV and DL; Investigation: BLAC, AQN, WWP, KWKC, ZS, SSL, MJGW, MMC, JGL, EEO, SV and DL; Writing: BLAC, AQN, SV, and DL with input from all authors.

Competing interests

Authors declare that they have no competing interests.

Data availability

The data that support this study are available from the corresponding authors upon reasonable request. The cryoEM density maps have been deposited in the Electron Microscopy Data Bank (EMDB) under accession codes EMD-36483 (isNS1ts:Fab56.2) and EMD-36480 (Fab56.2:isNS1ts:HDL). The protein model files for isNS1ts:Fab56.2 and Fab56.2:isNS1ts:HDL model are available upon request. Crosslinking MS raw files and the search results can be downloaded from *https://repository.jpostdb.org/preview/14869768463bf85b347ac2* with the access code: 3827. The HDX-MS data is deposited to the ProteomeXchange consortium via PRIDE partner repository[51] with the dataset identifier PXD042235.

References

1 Bhatt S., et al. (2013) **The global distribution and burden of dengue** *Nature* **496**:504–507 https://doi.org/10.1038/nature12060

2 Diamond M. S., Pierson T. C (2015) **Molecular Insight into Dengue Virus Pathogenesis and Its Implications for Disease Control** *Cell* **162**:488–492 https://doi.org/10.1016/j.cell.2015.07.005

3 Libraty D. H., et al. (2002) **High Circulating Levels of the Dengue Virus Nonstructural Protein NS1 Early in Dengue Illness Correlate with the Development of Dengue Hemorrhagic Fever** *J Infect Dis* **186**:1165–1168 https://doi.org/10.1086/343813

4 Paranavitane S. A., et al. (2014) **Dengue NS1 antigen as a marker of severe clinical disease** *BMC Infect Dis* **14** https://doi.org/10.1186/s12879-014-0570-8

5 Glasner D. R., Puerta-Guardo H., Beatty P. R., Harris E (2018) **The Good, the Bad, and the Shocking: The Multiple Roles of Dengue Virus Nonstructural Protein 1 in Protection and Pathogenesis** *Annu Rev Virol* **5**:227–253 https://doi.org/10.1146/annurev-virology-101416-041848

6 Watterson D., Modhiran N., Young P. R (2016) **The many faces of the flavivirus NS1 protein offer a multitude of options for inhibitor design** *Antiviral Res* **130**:7–18 https://doi.org/10.1016/j.antiviral.2016.02.014

7 Scaturro P., Cortese M., Chatel-Chaix L., Fischl W., Bartenschlager R (2015) **Dengue Virus Non-structural Protein 1 Modulates Infectious Particle Production via Interaction with the Structural Proteins** *PLOS Pathogens* **11** https://doi.org/10.1371/journal.ppat.1005277

8 Plaszczyca A., et al. (2019) **A novel interaction between dengue virus nonstructural protein 1 and the NS4A-2K-4B precursor is required for viral RNA replication but not for formation of the membranous replication organelle** *PLoS Pathog* **15** https://doi.org/10.1371/journal.ppat.1007736

9 Puerta-Guardo H., Glasner D. R., Harris E (2016) **Dengue Virus NS1 Disrupts the Endothelial Glycocalyx, Leading to Hyperpermeability** *PLoS Pathog* **12** https://doi.org/10.1371/journal.ppat.1005738

10 Beatty P. R., et al. (2015) **Dengue virus NS1 triggers endothelial permeability and vascular leak that is prevented by NS1 vaccination** *Sci Transl Med* **7**:304–141 https://doi.org/10.1126/scitranslmed.aaa3787

11 Akey D. L., et al. (2014) **Flavivirus NS1 Structures Reveal Surfaces for Associations with Membranes and the Immune System** *Science* **343**:881–885 https://doi.org/10.1126/science.1247749

12 Xu X., et al. (2016) **Contribution of intertwined loop to membrane association revealed by Zika virus full-length NS1 structure** *EMBO J* **35**:2170–2178 https://doi.org/10.15252/embj.201695290

13 Brown W. C., et al. (2016) **Extended surface for membrane association in Zika virus NS1 structure** *Nature Structural & Molecular Biology* **23**:865–867 https://doi.org/10.1038/nsmb.3268

14 Flamand M., et al. (1999) **Dengue Virus Type 1 Nonstructural Glycoprotein NS1 Is Secreted from Mammalian Cells as a Soluble Hexamer in a Glycosylation-Dependent Fashion** *Journal of Virology* **73**:6104–6110 https://doi.org/10.1128/JVI.73.7.6104-6110.1999

15 Gutsche I., et al. (2011) **Secreted dengue virus nonstructural protein NS1 is an atypical barrel-shaped high-density lipoprotein** *Proc Natl Acad Sci U S A* **108**:8003–8008 https://doi.org/10.1073/pnas.1017338108

16 Muller D. A., et al. (2012) **Structure of the dengue virus glycoprotein non-structural protein 1 by electron microscopy and single-particle analysis** *J Gen Virol* **93**:771–779 https://doi.org/10.1099/vir.0.039321-0

17 Shu B., et al. (2022) **CryoEM structures of the multimeric secreted NS1, a major factor for dengue hemorrhagic fever** *Nature Communications* **13** https://doi.org/10.1038/s41467-022-34415-1

18 Benfrid S., et al. (2022) **Dengue virus NS1 protein conveys pro-inflammatory signals by docking onto high-density lipoproteins** *EMBO Rep* **23** https://doi.org/10.15252/embr.202153600

19 Alcala A. C., et al. (2022) **Dengue Virus NS1 Uses Scavenger Receptor B1 as a Cell Receptor in Cultured Cells** *J Virol* **96** https://doi.org/10.1128/JVI.01664-21

20 Avirutnan P., et al. (2007) **Secreted NS1 of dengue virus attaches to the surface of cells via interactions with heparan sulfate and chondroitin sulfate E** *PLoS Pathog* **3** https://doi.org/10.1371/journal.ppat.0030183

21 Alcala A. C., et al. (2017) **The dengue virus non-structural protein 1 (NS1) is secreted from infected mosquito cells via a non-classical caveolin-1-dependent pathway** *J Gen Virol* **98**:2088–2099 https://doi.org/10.1099/jgv.0.000881

22 Rodriguez-Roche R., et al. (2005) **Virus evolution during a severe dengue epidemic in Cuba, 1997** *Virology* **334**:154–159 https://doi.org/10.1016/j.virol.2005.01.037

23 Chan K. W. K., et al. (2019) **A T164S mutation in the dengue virus NS1 protein is associated with greater disease severity in mice** *Sci Transl Med* **11** https://doi.org/10.1126/scitranslmed.aat7726

24 Kitti C. W. K (2019) **THE ROLE OF GENETIC VARIANTS OF NON-STRUCTURAL PROTEIN 1 IN DENGUE PATHOGENESIS**

25 Wu S., et al. (2012) **Fabs enable single particle cryoEM studies of small proteins** *Structure (London, England : 1993)* **20**:582–592 https://doi.org/10.1016/j.str.2012.02.017

26 Bloch J. S., et al. (2020) **Structure and mechanism of the ER-based glucosyltransferase ALG6** *Nature* **579**:443–447 https://doi.org/10.1038/s41586-020-2044-z

27 Jumper J., et al. (2021) **Highly accurate protein structure prediction with AlphaFold** *Nature* **596**:583–589 https://doi.org/10.1038/s41586-021-03819-2

28 Mirdita M., et al. (2022) **ColabFold: making protein folding accessible to all** *Nature Methods* **19**:679–682 https://doi.org/10.1038/s41592-022-01488-1

29 Biering S. B., et al. (2021) **Structural basis for antibody inhibition of flavivirus NS1-triggered endothelial dysfunction** *Science* **371**:194–200 https://doi.org/10.1126/science.abc0476

30 Silva R. A., et al. (2008) **Structure of apolipoprotein A-I in spherical high density lipoproteins of different sizes** *Proc Natl Acad Sci U S A* **105**:12176–12181 https://doi.org/10.1073/pnas.0803626105

31 He Y., et al. (2019) **Apolipoprotein A1 Forms 5/5 and 5/4 Antiparallel Dimers in Human High-density Lipoprotein** *Molecular & Cellular Proteomics* **18**:854–864 https://doi.org/10.1074/mcp.RA118.000878

32 Kao A., et al. (2011) **Development of a Novel Cross-linking Strategy for Fast and Accurate Identification of Cross-linked Peptides of Protein Complexes** *Molecular & Cellular Proteomics* **10** https://doi.org/10.1074/mcp.M110.002212

33 Edeling M. A., Diamond M. S., Fremont D. H (2014) **Structural basis of Flavivirus NS1 assembly and antibody recognition** *Proc Natl Acad Sci U S A* **111**:4285–4290 https://doi.org/10.1073/pnas.1322036111

34 Modhiran N., et al. (2021) **A broadly protective antibody that targets the flavivirus NS1 protein** *Science* **371**:190–194 https://doi.org/10.1126/science.abb9425

35 Wang D., et al. (2017) **A Mutation Identified in Neonatal Microcephaly Destabilizes Zika Virus NS1 Assembly in Vitro** *Sci Rep* **7** https://doi.org/10.1038/srep42580

36 Poonsiri T., et al. (2018) **Structural Study of the C-Terminal Domain of Nonstructural Protein 1 from Japanese Encephalitis Virus** *J Virol* **92** https://doi.org/10.1128/jvi.01868-17

37 Low J. G., et al. (2014) **Efficacy and safety of celgosivir in patients with dengue fever (CELADEN): a phase 1b, randomised, double-blind, placebo-controlled, proof-of-concept trial** *The Lancet Infectious Diseases* **14**:706–715 https://doi.org/10.1016/s1473-3099(14)70730-3

38 Young P. R., Hilditch P. A., Bletchly C., Halloran W (2000) **An Antigen Capture Enzyme-Linked Immunosorbent Assay Reveals High Levels of the Dengue Virus Protein NS1 in the Sera of Infected Patients** *Journal of Clinical Microbiology* **38**:1053–1057 https://doi.org/10.1128/jcm.38.3.1053-1057.2000

39 Alcon S., et al. (2002) **Enzyme-Linked Immunosorbent Assay Specific to Dengue Virus Type 1 Nonstructural Protein NS1 Reveals Circulation of the Antigen in the Blood during the Acute Phase of Disease in Patients Experiencing Primary or Secondary Infections** *Journal of Clinical Microbiology* **40**:376–381 https://doi.org/10.1128/jcm.40.02.376-381.2002

40 Malajczuk C. J., Gandhi N. S., Mancera R. L (2021) **Structure and intermolecular interactions in spheroidal high-density lipoprotein subpopulations** *J Struct Biol X* **5** https://doi.org/10.1016/j.yjsbx.2020.100042

41 Puerta-Guardo H., et al. (2019) **Flavivirus NS1 Triggers Tissue-Specific Vascular Endothelial Dysfunction Reflecting Disease Tropism** *Cell Rep* **26**:1598–1613 https://doi.org/10.1016/j.celrep.2019.01.036

42 Trinder M., Walley K. R., Boyd J. H., Brunham L. R (2020) **Causal Inference for Genetically Determined Levels of High-Density Lipoprotein Cholesterol and Risk of Infectious Disease. Arteriosclerosis** *Thrombosis, and Vascular Biology* **40**:267–278 https://doi.org/10.1161/ATVBAHA.119.313381

43 Tall A. R (2020) **HDL in Morbidity and Mortality: A 40+ Year Perspective** *Clinical Chemistry* **67**:19–23 https://doi.org/10.1093/clinchem/hvaa148

44 Harslof M., Pedersen K. M., Afzal S., Davey Smith G., Nordestgaard B. G (2023) **Lower levels of small HDL particles associated with increased infectious disease morbidity and mortality: a population-based cohort study of 30 195 individuals** *Cardiovasc Res* **119**:957–968 https://doi.org/10.1093/cvr/cvac194

45 Acton S., et al. (1996) **Identification of scavenger receptor SR-BI as a high density lipoprotein receptor** *Science* **271**:518–520 https://doi.org/10.1126/science.271.5248.518

46 Alcon-LePoder S., et al. (2005) **The Secreted Form of Dengue Virus Nonstructural Protein NS1 Is Endocytosed by Hepatocytes and Accumulates in Late Endosomes: Implications for Viral Infectivity** *Journal of Virology* **79**:11403–11411 https://doi.org/10.1128/jvi.79.17.11403-11411.2005

47 Wang C., et al. (2019) **Endocytosis of flavivirus NS1 is required for NS1-mediated endothelial hyperpermeability and is abolished by a single N-glycosylation site mutation** *PLoS Pathog* **15** https://doi.org/10.1371/journal.ppat.1007938

48 Modhiran N., et al. (2015) **Dengue virus NS1 protein activates cells via Toll-like receptor 4 and disrupts endothelial cell monolayer integrity** *Sci Transl Med* **7** https://doi.org/10.1126/scitranslmed.aaa3863

49 Coelho D. R., et al. (2021) **ApoA1 Neutralizes Proinflammatory Effects of Dengue Virus NS1 Protein and Modulates Viral Immune Evasion** *J Virol* **95** https://doi.org/10.1128/JVI.01974-20

50 Lee P. X., et al. (2020) **Relative contribution of nonstructural protein 1 in dengue pathogenesis** *J Exp Med* **217** https://doi.org/10.1084/jem.20191548

51 Perez-Riverol Y., et al. (2021) **The PRIDE database resources in 2022: a hub for mass spectrometry-based proteomics evidences** *Nucleic Acids Research* **50**:D543–D552 https://doi.org/10.1093/nar/gkab1038

Article and author information

Bing Liang Alvin Chew

Lee Kong Chian School of Medicine, Nanyang Technological University; EMB 03-07, 59 Nanyang Drive, Singapore 636921, NTU Institute of Structural Biology, Nanyang Technological University; EMB 06-01, 59 Nanyang Drive, Singapore 636921, Singapore
ORCID iD: 0000-0002-2748-9366

An Qi Ngoh

Program in Emerging Infectious Diseases, Duke-NUS Medical School; 8 College Road, Singapore 169857, Singapore

Wint Wint Phoo
Functional Proteomics Laboratory, Institute of Molecular and Cell Biology, Agency for Science, Technology and Research (A*STAR); 61 Biopolis Drive, Proteos, Singapore 138673, Singapore

Kitti Wing Ki Chan
Program in Emerging Infectious Diseases, Duke-NUS Medical School; 8 College Road, Singapore 169857, Singapore

Zheng Ser
Functional Proteomics Laboratory, Institute of Molecular and Cell Biology, Agency for Science, Technology and Research (A*STAR); 61 Biopolis Drive, Proteos, Singapore 138673, Singapore

Nikhil K Tulsian
Department of Biological Sciences, National University of Singapore, Singapore, Singapore
Centre for Life Sciences, Department of Biochemistry, National University of Singapore, Singapore, Singapore

Shiao See Lim
Program in Emerging Infectious Diseases, Duke-NUS Medical School; 8 College Road, Singapore 169857, Singapore

Mei Jie Grace Weng
Lee Kong Chian School of Medicine, Nanyang Technological University; EMB 03-07, 59 Nanyang Drive, Singapore 636921, NTU Institute of Structural Biology, Nanyang Technological University; EMB 06-01, 59 Nanyang Drive, Singapore 636921, Singapore

Satoru Watanabe
Program in Emerging Infectious Diseases, Duke-NUS Medical School; 8 College Road, Singapore 169857, Singapore

Milly M. Choy
Program in Emerging Infectious Diseases, Duke-NUS Medical School; 8 College Road, Singapore 169857, Singapore

Jenny G. Low
Program in Emerging Infectious Diseases, Duke-NUS Medical School; 8 College Road, Singapore 169857, Singapore, Department of Infectious Diseases, Singapore General Hospital, Singapore, Singapore

Eng Eong Ooi
Program in Emerging Infectious Diseases, Duke-NUS Medical School; 8 College Road, Singapore 169857, Singapore, Yong Loo Lin School of Medicine, National University of Singapore, Singapore, Singapore, Saw Swee Hock School of Public Health, National University of Singapore, Singapore, Singapore

Christiane Ruedl
School of Biological Sciences, Nanyang Technological University, Singapore, Singapore

Radoslaw M. Sobota
Functional Proteomics Laboratory, Institute of Molecular and Cell Biology, Agency for Science, Technology and Research (A*STAR); 61 Biopolis Drive, Proteos, Singapore 138673, Singapore

Subhash G. Vasudevan
Program in Emerging Infectious Diseases, Duke-NUS Medical School; 8 College Road, Singapore 169857, Singapore, Department of Microbiology and Immunology, National University of Singapore; 5 Science Drive 2, Singapore 117545, Singapore, Institute for Glycomics (G26), Griffith University Gold Coast Campus, QLD 4222, Australia
For correspondence: subhash.vasudevan@duke-nus.edu.sg
ORCID iD: 0000-0002-5083-3831

Dahai Luo
Lee Kong Chian School of Medicine, Nanyang Technological University; EMB 03-07, 59 Nanyang Drive, Singapore 636921, NTU Institute of Structural Biology, Nanyang Technological University; EMB 06-01, 59 Nanyang Drive, Singapore 636921, Singapore
For correspondence: luodahai@ntu.edu.sg
ORCID iD: 0000-0001-7637-7275

Copyright

Editors

Reviewing Editor
Neil Ferguson
Imperial College London, London, United Kingdom

Senior Editor
Detlef Weigel
Max Planck Institute for Biology Tübingen, Tübingen, Germany

Reviewer #1 (Public Review):

The authors of this study seek to visualize NS1 purified from dengue virus infected cells. They infect vero cells with DV2-WT and DV2 NS1-T164S (a mutant virus previously characterized by the authors). The authors utilize an anti-NS1 antibody to immunoprecipitate NS1 from cell supernatants and then elute the antibody/NS1 complex with acid. The authors evaluate the eluted NS1 by SDS-PAGE, Native Page, mass spec, negative-stain EM, and eventually Cryo-EM. SDS-PAGE, mas spec, and native page reveal a >250 Kd species containing both NS1 and the proteinaceous component of HDL (ApoA1). The authors produce evidence to suggest that this population is predominantly NS1 in complex with ApoA1. This contrasts with recombinantly produced NS1 (obtained from a collaborator) which did not appear to be in complex with or contain ApoA1 (Figure 1C). The authors then visualize their NS1 stock in complex with their monoclonal antibody by CryoEM. For NS1-WT, the major species visualized by the authors was a ternary complex of an HDL particle in complex with an NS1 dimer bound to their mAB. For their mutant NS1-T164S, they find similar structures, but in contrast to NS1-WT, they visualize free NS1 dimers in complex with 2 Fabs (similar to what's been reported previously) as one of the major species. This highlights that different NS1 species have markedly divergent structural dynamics. It's important to note that the electron density maps for their structures do appear to be a bit overfitted since there are many regions with electron density that do not have a predicted fit and their HDL structure does not appear to have any

predicted secondary structure for ApoA1. The authors then map the interaction between NS1 and ApoA1 using cross-linking mass spectrometry revealing numerous NS1-ApoA1 contact sites in the beta-roll and wing domain. The authors find that NS1 isolated from DENV infected mice is also present as a >250 kD species containing ApoA1. They further determine that immunoprecipitation of ApoA1 out of the sera from a single dengue patient correlates with levels of NS1 (presumably COIPed by ApoA1) in a dose-dependent manner.

In the end, the authors make some useful observations for the NS1 field (mostly confirmatory) providing additional insight into the propensity of NS1 to interact with HDL and ApoA1. The study does not provide any functional assays to demonstrate activity of their proteins or conduct mutagenesis (or any other assays) to support their interaction predications. The authors assertion that higher-order NS1 exists primarily as a NS1 dimer in complex with HDL is not well supported as their purification methodology of NS1 likely introduces bias as to what NS1 complexes are isolated. While their results clearly reveal NS1 in complex with ApoA1, the lack of other NS1 homo-oligomers may be explained by how they purify NS1 from virally infected supernatant. Because NS1 produced during viral infection is not tagged, the authors use an anti-NS1 monoclonal antibody to purify NS1. This introduces a source of bias since only NS1 oligomers with their mAb epitope exposed will be purified. Further, the use of acid to elute NS1 may denature or alter NS1 structure and the authors do not include controls to test functionality of their NS1 stocks (capacity to trigger endothelial dysfunction or immune cell activation). The acid elution may force NS1 homo-oligomers into dimers which then reassociate with ApoA1 in a manner that is not reflective of native conditions. Conducting CryoEM of NS1 stocks only in the presence of full-length mAbs or Fabs also severely biases what species of NS1 is visualized since any NS1 oligomers without the B-ladder domain exposed will not be visualized. If the residues obscured by their mAb are involved in formation of higher-order oligomers then this antibody would functionally inhibit these species from forming. The absence of critical controls, use of one mAb, and acid elution for protein purification severely limits the interpretation of these data and do not paint a clear picture of if NS1 produced during infection is structurally distinct from recombinant NS1. Certainly there is novelty in purifying NS1 from virally infected cells, but without using a few different NS1 antibodies to purify NS1 stocks (or better yet a polyclonal population of antibodies) it's unclear if the results of the authors are simply a consequence of the mAb they selected.

Data produced from numerous labs studying structure and function of flavivirus NS1 proteins provide diverse lines of evidence that the oligomeric state of NS1 is dynamic and can shift depending on context and environment. This means that the methodology used for NS1 production and purification will strongly impact the results of a study. The data in this manuscript certainly capture one of these dynamic states and overall support the general model of a dynamic NS1 oligomer that can associate with both host proteins as well as itself but the assertions of this manuscript are overall too strong given their data, as there is little evidence in this manuscript, and none available in the large body of existing literature, to support that NS1 exists only as a dimer associated with ApoA1. More likely the results of this paper are a result of their NS1 purification methodology.

Comments on revised version:

The authors have not adequately addressed my concerns from the original review. My major concerns are that the binding modality of NS1 to ApoA1/HDL was not validated using a mutagenesis approach and that the overarching conclusion drawn by the authors, that the major species of NS1 in vivo is a dimer in complex with ApoA1, is not supported by the data in this study given the methodology of using a single monoclonal antibody to immunoprecipitate NS1. Certainly, the structures in this manuscript are valuable in confirming that NS1 interacts with HDL and captures a snapshot of NS1/HDL interaction dynamics, but the use of only a single antibody is a major source of bias that makes it

challenging to draw conclusions about the oligomeric state of NS1. Further on this point, a critically important control that is missing from this study is to determine if the anti-NS1 mAb 56.2 prevents NS1 from interacting with cells, triggering the release of proinflammatory cytokines from immune cells, or mediating endothelial dysfunction of endothelial cells. If this antibody inhibits these NS1-triggered events (linked to pathogenesis), it would suggest that the NS1 within this ternary complex is not active. Presumably some protective anti-NS1 antibodies may function by modulating the oligomeric state of NS1.

https://doi.org/10.7554/eLife.90762.2.sa1

Reviewer #2 (Public Review):

Summary:

Chew et al describe interaction of the flavivirus protein NS1 with HDL using primarily cryoEM and mass spec. The NS1 was secreted from dengue virus infected Vero cells, and the HDL were derived from the 3% FBS in the culture media. NS1 is a virulence factor/toxin and is a biomarker for dengue infection in patients. The mechanisms of its various activities in the host are incompletely understood. NS1 has been seen in dimer, tetramer and hexamer forms. It is well established to interact with membrane surfaces, presumably through a hydrophobic surface of the dimer form, and the recombinant protein has been shown to bind HDL. In this study, cryoEM and crosslinking-mass spec are used to examine NS1 secreted from virus-infected cells, with the conclusion that the sNS1 is predominantly/exclusively HDL-associated through specific contacts with the ApoA1 protein.

Strengths: The experimental results are consistent with previously published data.

Weaknesses:

CryoEM:
Some of the neg-stain 2D class averages for sNS1 in Fig S1 clearly show 1 or 2 NS1 dimers on the surface of a spherical object, presumably HDL, and indicate the possibility of high-quality cryoEM results. However, the cryoEM results are disappointing. The cryo 2D class averages and refined EM map in Fig S4 are of poor quality, indicating sub-optimal grid preparation or some other sample problem. Some of the FSC curves (2 in Fig S7 and 1 in Fig S6) have extremely peculiar shapes, suggesting something amiss in the map refinement. The sharp drop in the "corrected" FSC curves in Figs S5c and S6c (upper) indicate severe problems. The stated resolutions (3.42 & 3.82 Å) for the sNS1ts-Fab56.2 are wildly incompatible with the images of the refined maps in Figs 3 & S7. At those resolutions, clear secondary structural elements should be visible throughout the map. From the 2D averages and 3D maps shown in the figures, this does not seem to be the case. Local resolution maps should be shown for each structure.

The samples were clearly challenging for cryoEM, leading to poor quality maps that were difficult to interpret. None of the figures are convincing that NS1, Ab56.2 or Fab56.2 are correctly fit into EM maps. There is no indication of ApoA1 helices. Details of the fit of models to density for key regions of the higher-resolution EM maps should be shown and the models should be deposited in the PDB. An example of modeling difficulty is clear in the sNS1ts dimer with bound Fab56.2 (figs 3c & S7e). For this complex, the orientation of the Fab56.2 relative to the sNS1ts dimer in this submission (Fig 3c) is substantially different than in the bioRxiv preprint (Fig 3c). Regions of empty density in Fig 3c also illustrate the challenge of building a model into this map.

Mass spec:
Crosslinking-mass spec was used to detect contacts between NS1 and ApoA1, providing strong

validation of the sNS1-HDL association. As the crosslinks were detected in a bulk sample, they show that NS1 is near ApoA1 in many/most HDL particles, but they do not indicate a specific protein-protein complex. Thus, the data do not support the model of an NS1-ApoA1 complex in Fig 4d. Further, a specific NS1-ApoA1 interaction should have evidence in the EM maps (helical density for ApoA1), but none is shown or mentioned. If such exists, it could perhaps be visualized after focused refinement of the map for sNS1ts-HDL with Fab56.2 (Fig S7d). The finding that sNS1-ApoA1 crosslinks involved residues on the hydrophobic surface of the NS1 dimer confirms previous data that this NS1 surface engages with membranes and lipids.

Sample quality:
The paper lacks any validation that the purified sNS1 retains established functions, for example the ability to enhance virus infectivity or to promote endothelial dysfunction. Peculiarities include the gel filtration profiles (Fig 2a), which indicate identical elution volumes (apparent MWs) for sNS1wt-HDL bound to Ab562 (~150 kDa) and to the ~3X smaller Fab56.2 (~50 kDa). There should also be some indication of sNS1wt-HDL pairs crosslinked by the full-length Ab, as can be seen in the raw cryoEM micrograph (Fig S5b).

Obtaining high quality structures is often more demanding of sample integrity than are activity assays. Given the low quality of the cryoEM maps, it's possible that the acidification step in immunoaffinity purification damaged the HDL complex. No validation of HDL integrity, for example with acid-treated HDL, is reported. Acid treatment is perhaps discounted by a statement (line 464) that another group also used immunoaffinity purification in a recent study (ref 20) reporting sNS1 bound to HDL. However the statement is incorrect; the cited study used affinity purification via a strep-tag on recombinant sNS1.

Discussion:
The Discussion reflects a view that the NS1 secreted from virus-infected cells is a 1:1 sNS1dimer:HDL complex with the specific NS1-ApoA1 contacts detected by crosslinking mass spec. This is inconsistent with both the neg-stain 2D class average with 2 sNS1 dimers on an HDL (Fig S1c) and with the recent study of Flamand & co-workers showing 1-3 NS1 dimers per HDL (ref 20). It also ignores the propensity of NS1 to associate with membranes and lipids. It is far more likely that NS1 association with HDL is driven by these hydrophobic interactions than by specific protein-protein contacts. A lengthy Discussion section (lines 461-522) includes several chemically dubious or inconsistent statements, all based on the assumption that specific ApoA1 contacts are essential to NS1 association with HDL and that sNS1 oligomers higher than the dimer necessarily involve ApoA1 interaction, conclusions that are not established by the data in this paper.

Additional comments on the revised manuscript:

Comments on the structures:

The authors kindly provided their fitted atomic models for the 2 reported structures. The EM maps are available in the EMDB. Based on these materials, the derived structures are not well supported due to problems with the models, the maps, and the fit of models to maps.

Quick inspection revealed that the models for both structures are implausible due to a large steric clash of Fab56.2 and the end of the NS1. The Fab and NS1 protein backbones interpenetrate by nearly 20 Å. This substantial overlap exists for all 3 Fab56.2-NS1 interactions in the 2 structures, and is also visible in the perpendicular views of the NS1 dimer with 2 bound Fab56.2 in Fig. 2c. It appears that the Fab56.2 model was jammed into the NS1 model in order to bring all domains inside the density envelope at the threshold chosen to display the map. The poor fit of model to map is also clear in several protruding density regions without any model.

The fits of both atomic models to the maps are questionable because
- The maps suffer from severe preferred orientation problems, as seen in the streaky tubes of

density. The streaks in both maps do not match the NS1 beta strands of the fitted models.
- The shape of the modeled ApoA1 helical ring surrounding the HDL does not match the shape of the EM density. In some regions, the ApoA1 helices are inside the rather strong density for the spherical HDL, but in other regions the helices are outside the density.
- Both maps have regions of strong density that are adjacent to NS1 but lack any protein model, while other parts of the structure, including the beta-roll domain, lack density.
- The claimed 4.3-Å resolution of the NS1-Fab56.2 complex is wildly overstated. The local resolution of ~2.5 Å for the "best" part of the structure (Supp Fig. 7E) appears to pertain to the beta strands at the center of the NS1 dimer. However, these density streaks do not match the beta strands of the fit model.
- The manuscript lacks statistics on the fit of model to map. A standard cryo-EM "Table 1" should include more than is presented in Supp Table 1. The fitted model for at least the higher resolution structure should be deposited in the PDB.

Comments on the structure interpretation:

By now it should be abundantly clear that the oligomer state of NS1 is dynamic and highly sensitive to environmental conditions and to each sample's "history". For the reasons pointed out by reviewer 1, it is not clear that the immunoaffinity purification method captured all forms of sNS1 equally. Thus, the authors insistence that NS1 secreted from virus-infected cells is predominantly bound to HDL particles in a ratio of 1 NS1 dimer per HDL is not well supported. They employ similar arguments to challenge the discovery of sNS1 as a lipoprotein particle (PNAS 2011), contending that the 2011 finding was an artefact of recombinant NS1 production and is irrelevant to sNS1 from a virus infection. The several published structures of NS1 oligomers reveal a large degree of asymmetry in dimer-dimer interaction, consistent with the ability of NS1 to dynamically associate with a variety of hydrophobic entities.

https://doi.org/10.7554/eLife.90762.2.sa0

Author Response

The following is the authors' response to the original reviews.

> ***Public Reviews:***
>
> ***Reviewer #1 (Public Review):***
>
> *The authors of this study seek to visualize NS1 purified from dengue virus infected cells. They infect vero cells with DV2-WT and DV2 NS1-T164S (a mutant virus previously characterized by the authors). The authors utilize an anti-NS1 antibody to immunoprecipitate NS1 from cell supernatants and then elute the antibody/NS1 complex with acid. The authors evaluate the eluted NS1 by SDS-PAGE, Native Page, mass spec, negative-stain EM, and eventually Cryo-EM. SDS-PAGE, mas spec, and native page reveal a >250 Kd species containing both NS1 and the proteinaceous component of HDL (ApoA1). The authors produce evidence to suggest that this population is predominantly NS1 in complex with ApoA1. This contrasts with recombinantly produced NS1 (obtained from a collaborator) which did not appear to be in complex with or contain ApoA1 (Figure 1C). The authors then visualize their NS1 stock in complex with their monoclonal antibody by CryoEM. For NS1-WT, the major species visualized by the authors was a ternary complex of an HDL particle in complex with an NS1 dimer bound to their mAB. For their mutant NS1-T164S, they find similar structures, but in contrast to NS1-WT, they visualize free NS1 dimers in complex with 2 Fabs (similar to what's been reported previously) as one of the major species. This highlights that different NS1 species have markedly divergent structural dynamics. It's important to note that the electron density*

maps for their structures do appear to be a bit overfitted since there are many regions with electron density that do not have a predicted fit and their HDL structure does not appear to have any predicted secondary structure for ApoA1. The authors then map the interaction between NS1 and ApoA1 using cross-linking mass spectrometry revealing numerous NS1-ApoA1 contact sites in the beta-roll and wing domain. The authors find that NS1 isolated from DENV infected mice is also present as a >250 kD species containing ApoA1. They further determine that immunoprecipitation of ApoA1 out of the sera from a single dengue patient correlates with levels of NS1 (presumably COIPed by ApoA1) in a dose-dependent manner.

In the end, the authors make some useful observations for the NS1 field (mostly confirmatory) providing additional insight into the propensity of NS1 to interact with HDL and ApoA1. The study does not provide any functional assays to demonstrate activity of their proteins or conduct mutagenesis (or any other assays) to support their interaction predications. The authors assertion that higher-order NS1 exists primarily as a NS1 dimer in complex with HDL is not well supported as their purification methodology of NS1 likely introduces bias as to what NS1 complexes are isolated. While their results clearly reveal NS1 in complex with ApoA1, the lack of other NS1 homo-oligomers may be explained by how they purify NS1 from virally infected supernatant. Because NS1 produced during viral infection is not tagged, the authors use an anti-NS1 monoclonal antibody to purify NS1. This introduces a source of bias since only NS1 oligomers with their mAb epitope exposed will be purified. Further, the use of acid to elute NS1 may denature or alter NS1 structure and the authors do not include controls to test functionality of their NS1 stocks (capacity to trigger endothelial dysfunction or immune cell activation). The acid elution may force NS1 homo-oligomers into dimers which then reassociate with ApoA1 in a manner that is not reflective of native conditions. Conducting CryoEM of NS1 stocks only in the presence of full-length mAbs or Fabs also severely biases what species of NS1 is visualized since any NS1 oligomers without the B-ladder domain exposed will not be visualized. If the residues obscured by their mAb are involved in formation of higher-order oligomers then this antibody would functionally inhibit these species from forming. The absence of critical controls, use of one mAb, and acid elution for protein purification severely limits the interpretation of these data and do not paint a clear picture of if NS1 produced during infection is structurally distinct from recombinant NS1. Certainly there is novelty in purifying NS1 from virally infected cells, but without using a few different NS1 antibodies to purify NS1 stocks (or better yet a polyclonal population of antibodies) it's unclear if the results of the authors are simply a consequence of the mAb they selected.

Data produced from numerous labs studying structure and function of flavivirus NS1 proteins provide diverse lines of evidence that the oligomeric state of NS1 is dynamic and can shift depending on context and environment. This means that the methodology used for NS1 production and purification will strongly impact the results of a study. The data in this manuscript certainly capture one of these dynamic states and overall support the general model of a dynamic NS1 oligomer that can associate with both host proteins as well as itself but the assertions of this manuscript are overall too strong given their data, as there is little evidence in this manuscript, and none available in the large body of existing literature, to support that NS1 exists only as a dimer associated with ApoA1. More likely the results of this paper are a result of their NS1 purification methodology.

Suggestions for the Authors:

Major:

(1) Because of the methodology used for NS1 purification, it is not clear from the data provided if NS1 from viral infection differs from recombinant NS1. Isolating NS1 from viral infection using a polyclonal antibody population would be better to answer their

questions. On this point, Vero cells are also not the best candidate for their NS1 production given these cells do not come from a human. A more relevant cell line like U937-DC-SIGN would be preferable.

We performed an optimization of sNS1 secretion from DENV infection in different cell lines (Author response image 1 below) to identify the best cell line candidate to obtain relatively high yield of sNS1 for the study. As shown in Author response image 1, the levels of sNS1 in the tested human cell lines Huh7 and HEK 293T were at least 3-5 fold lower than in Vero cells. Although using a monocytic cell line expressing DC-SIGN as suggested by the reviewer would be ideal, in our experience the low infectivity of DENV in monocytic cell lines will not yield sufficient amount of sNS1 needed for structural analysis. For these practical reasons we decided to use the closely related non-human primate cell line Vero for sNS1 production supported by our optimization data.

Author response image 1.

sNS1 secretion in different mammalian and mosquito cell lines after DENV2 infection. The NS1 secretion level is measured using PlateliaTM Dengue NS1 Ag ELISA kit (Bio-Rad) on day 3 (left) and day 5 (right) post infection respectively.

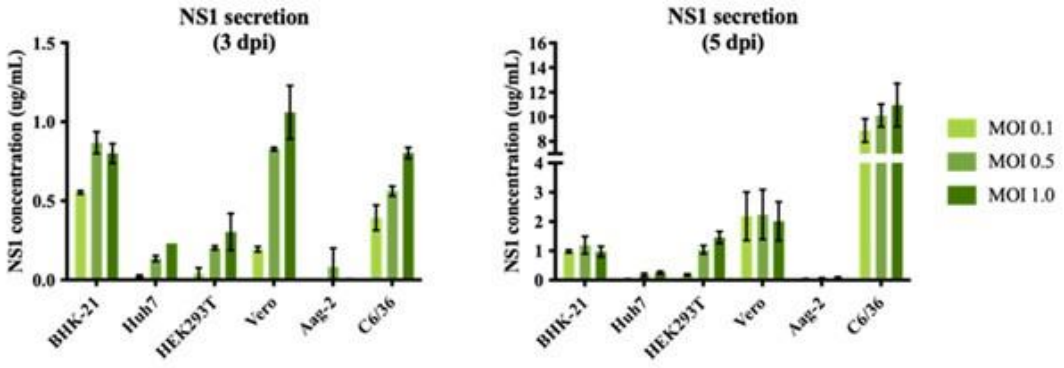

(2) The authors need to support their interaction predictions and models via orthogonal assays like mutagenesis followed by HDL/ApoA1 complexing and even NS1 functional assays. The authors should be able to mutate NS1 at regions predicted to be critical for ApoA1/HDL interaction. This is critical to support the central conclusions of this manuscript.

In our previous publication (Chan et al., 2019 Sci Transl Med), we used similarly purified sNS1 (immunoaffinity purification followed by acid elution) from infected culture supernatants from both DENV2 wild-type and T164S mutant (both also studied in the present work) to carry out stimulation assay on human PBMCs as described by other leading laboratories investigating NS1 (Modhiran et al., 2015 Sci Transl Med). For reader convenience we have extracted the data from our published paper and present it as Author response image 2 below.

Author response image 2.

(A) IL6 and (B) TNFa concentrations measured in the supernatants of human PBMCs incubated with either 1μg/ml or 10μg/ml of the BHK-21 immunoaffinity-purified WT and TS mutant sNS1 for 24 hours. Data is adapted from Chan et al., 2019.

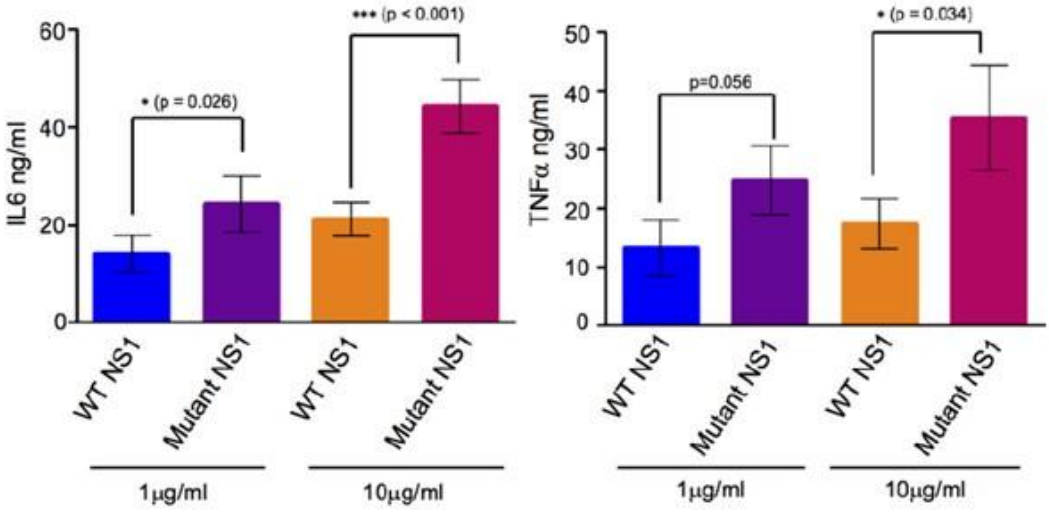

Incubation of immunoaffinity-purified sNS1 (WT and TS) with human PBMCs from 3 independent human donors triggered the production of proinflammatory cytokines IL6 and TNF in a concentration dependent manner (Author response image 2), consistent with the published data by Modhiran et al., 2015 Sci Transl Med. Interestingly the TS mutant derived sNS1 induced a higher proinflammatory cytokines production than WT virus derived sNS1 that appears to correlate with the more lethal and severe disease phenotype in mice as also reported in our previous work (Chan et al., 2019). Additionally, the functionality of our immune-affinity purified infection derived sNS1 (isNA1) is now further supported by our preliminary results on the NS1 induced endothelial cell permeability assay using the purified WT and mutant isNS1 (Author response image 3). As shown in Author response image 3, both the isNS1wt and isNS1ts mutant reduced the relative transendothelial resistance from 0 to 9 h post-treatment, with the peak resistance reduction observed at 6 h post-treatment, suggesting that the purified isNS1 induced endothelial dysfunction as reported in Puerta-Guardo et al., 2019, Cell Rep.) It is noteworthy that the isNS1 in our study behaves similarly as the commercial recombinant sNS1 (rsNS1 purchased from the same source used in study by Puerta-Guardo et al., 2019) in inducing endothelial hyperpermeability. Collectively our previous published and current data suggest that the purified isNS1 (as a complex with ApoA1) has a pathogenic role in disease pathogenesis that is also supported in a recent publication by Benfrid et al., EMBO 2022). The acid elution has not affected the functionality of NS1.

Author response image 3.

Functional assessment of isNS1wt and isNS1ts on vascular permeability in vitro. A trans-endothelial permeabilty assay via measurement of the transendothelial electrical resistance (TEER) on human umbilical vascular endothelial cells (hUVEC) was performed, as described previously (Puerta-Guardo et al., 2019, Cell Rep). Ovalbumin serves as the negative control, while TNF-α and rsNS1 serves as the positive controls.

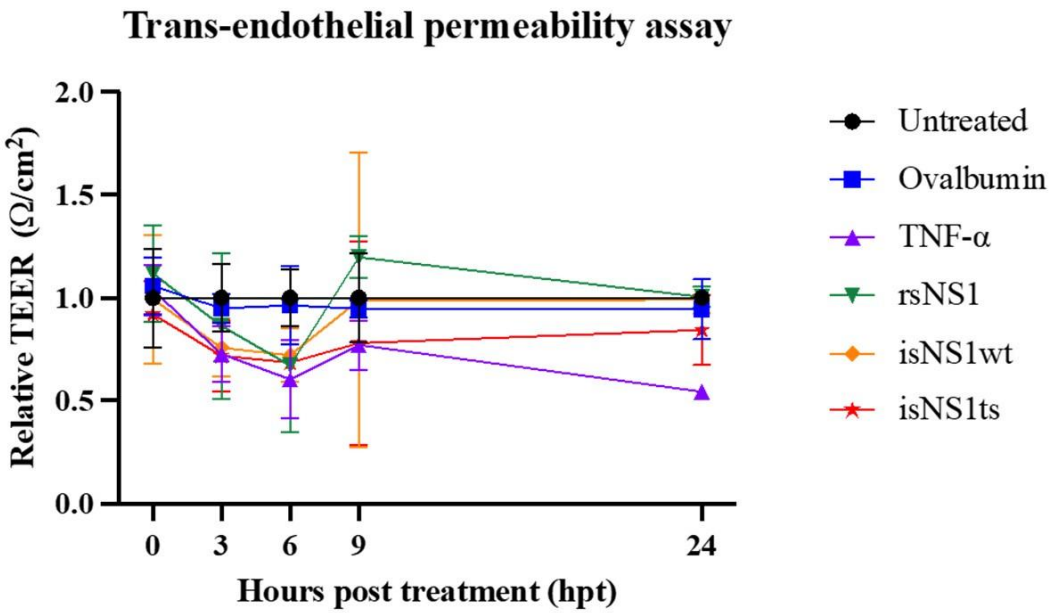

We agree with reviewer about the suggested mutagnesis study. We will perform site-directed mutagenesis at selected residues and further structural and functional analyses and report the results in a follow-up study.

> *(3) The authors need to show that the NS1 stocks produced using acid elution are functional compared to standard recombinantly produced NS1. Do acidic conditions impact structure/function of NS1?*

We are providing the same response to comments 1 & 2 above. We would like to reiterate that we have previously used sNS1 from immunoaffinity purification followed by acid elution to test its function in stimulating PBMCs to produce pro-inflammatory cytokines (Chan et al., 2019; Author response image 2). Similar to Modhiran et al. (2015) and Benfrid et al. (2022), the sNS1 that we extracted using acid elution are capable of activating PBMCs to produce pro-inflammatory cytokines. We have now further demonstrated the ability of both WT and TS isNS1 in inducing endothelial permeability in vitro in hUVECs, using the TEER assay (Author response image 3). Based on the data presented in the rebuttal figures as well as our previous publication we do not think that the acid elution has a significant impact on function of isNS1.

We performed affinity purification to enrich the complex for better imaging and analysis (Supp Fig. 1b) since the crude supernatant contains serum proteins and serum-free infections also do not provide sufficient isNS1. The major complex observed in negative stain is 1:1 (also under acidic conditions which implies that the complex are stable and intact). We agree that it is possible that other oligomers can form but we have observed only a small population (74 out of 3433 particles, 2.15%; 24 micrographs) of HDL:sNS1 complex at 1:2 ratio as shown in the Author response image 4 below and in the manuscript (p. 4 lines 114-117, Supp Fig. 1c). Other NS1 dimer:HDL ratios including 2:1 and 3:1 have been reported by Benfrid et al., 2022 by spiking healthy sera with recombinant sNS1 and subsequent re-affinity purification. However, this method used an approximately 8-fold higher sNS1 concentration (400 ug/mL) than the maximum clinically reported concentration (50 ug/mL) (Young et al., 2000; Alcon et al., 2002; Libraty et al., 2002). In our hands, the sNS1 concentration in the concentrated media from in vitro infection was quantified as 30 ug/mL which is more physiologically relevant.

We conclude that the integrity of the HDL of the complex is not lost during sample preparation, as we are able to observe the complex under the negative staining EM as well as infer from XL-MS. Our rebuttal data and our previous studies with our acid-eluted isNS1 from immunoaffinity purification clearly show that our protein is functional and biologically relevant.

Author response image 4.

(A) Representative negative stain micrograph of sNS1wt (B) Representative 2D averages of negative stained isNS1wt. Red arrows indicating the characteristic wing-like protrusions of NS1 inserted in HDL. (C) Data adapted from Figure 2 in Benfrid et al. (2022).

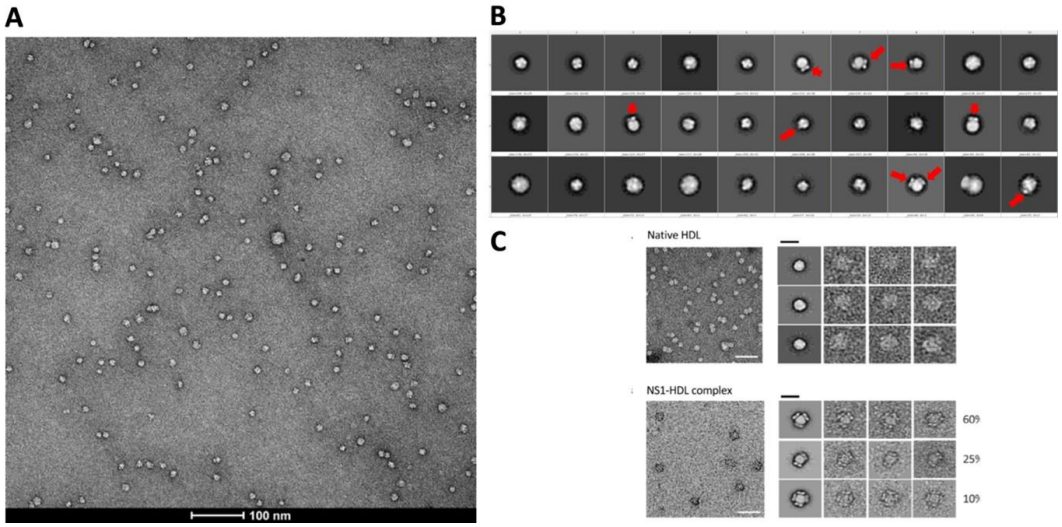

> *(4) Overall, the data obtained from the mutant NS1 (contrasted to WT NS1) reveals how dynamic the oligomeric state of NS1 proteins are but the authors do not provide any insight into how/why this is, some additional lines of evidence using either structural studies or mutagenesis to compare WT and their mutant and even NS1 from a different serotype of DENV would help the field to understand the dynamic nature of NS1.*

The T164S mutation in DENV2 NS1 was proposed as the residue associated with disease severity in 1997 Cuban dengue epidemic (Halsted SB. “Intraepidemic increases in dengue disease severity: applying lessons on surveillance and transmission”. Whitehorn, J., Farrar. J., Eds., Clinical Insights in Dengue: Transmission, Diagnosis & Surveillance. The Future Medicine (2014), pp. 83-101). Our previous manuscript examined this mutation by engineering it into a less virulent clade 2 DENV isolated in Singapore and showed that sNS1 production was higher without any change in viral RNA replication. Transcript profiling of mutant compared to WT virus showed that genes that are usually induced during vascular leakage were upregulated for the mutant. We also showed that infection of interferon deficient AG129 mice with the mutant virus resulted in disease severity, increased complement protein expression in the liver, tissue inflammation and greater mortality compared to WT virus infected mice. The lipid profiling in our study (Chan et al., 2019) suggested small differences with WT but was overall similar to HDL as described by Gutsche et al. (2011). We were intrigued by our functional results and wanted to explore more deeply the impact of the mutation on sNS1 structure which at that stage was widely believed to be a trimer of NS1 dimers with a central channel (~ X Å) stuffed with lipid as established in several seminal publications (Flamand et al., 1999; Gutsche et al., 2011; Muller et al., 2012). In fact “This Week in Virology” netcast (https://www.microbe.tv/twiv/twiv-725/) discussed two back-

to-back publications in Science (Modhiran et al., 371(6625)190-194; Biering et al., Science 371(6625):194-200)) which showed that therapeutic antibodies can ameliorate the NS1 induced pathogenesis and expert discussants posed questions that also pointed to the need for more accurate definition of the molecular composition and architecture of the circulating NS1 complex during virus infection to get a clearer handle on its pathogenic mechanism. Our current studies and also the recent high resolution cryoEM structures (Shu et al., 2022) do not support the notion of a central channel "stuffed with lipid". Even in the rare instances where trimer of dimers are shown, the narrow channel in the center could only accommodate one molecule of lipoid molecule no bigger than a typical triglyceride molecule. This hexamer model cannot explain the lipid proeotmics data in the literature.

In our study we observed predominantly 1:1 NS1 dimer to HDL (~30 µg/mL) mirroring maximum clinically reported concentration of sNS1 in the sera of DENV patients (40-50 µg/mL) as we highlighted in our main text (P. 18, lines 461-471). What is often quoted (also see later) is the recent study of Flamand & co-workers which show 1-3 NS1 dimers per HDL (Benfrid et al, 2022) by spiking rsNS1 (400 µg/mL) with HDL. This should not be confused with the previous models which suggested a lipid filled central channel holding together the hexamer. The use of physiologically relevant concentrations is important for these studies as we have highlighted in our main text (P. 18, lines 461-471).

Our interpretation for the mutant (isNS1ts) is that it is possible that the hydrophilic serine at residue 164 located in the greasy finger loop may weaken the isNS1ts binding to HDL hence the observation of free sNS1 dimers in our immunoaffinity purified (acid eluted sample). The disease severity and increased complement protein expression in AG129 mice liver can be ascribed to weakly bound mutant NS1 with fast on/off rate with HDL being transported to the liver where specific receptors bind to free sNS1 and interact with effector proteins such as complement to drive inflammation and associated pathology. Our indirect support for this is that the XL-MS analysis of purified isNS1ts identified only 7 isNS1ts:ApoA1 crosslinks while 25 isNS1wt:ApoA1 crosslinks were identified from purified isNS1wt (refer to Fig. 4 and Supp. Fig. 8).

Taken together, the cryoEM and XL-MS analysis of purified isNS1ts suggest that isNS1ts has weaker affinity for HDL compared to isNS1wt. We welcome constructive discussion on our interpretation that we and others will hopefully obtain more data to support or deny our proposed explanation. Our focus has been to compare WT with mutant sNS1 from DENV2 and we agree that it will be useful to study other serotypes.

> ***Reviewer #2:***
>
> *CryoEM:*
>
> *Some of the neg-stain 2D class averages for sNS1 in Fig S1 clearly show 1 or 2 NS1 dimers on the surface of a spherical object, presumably HDL, and indicate the possibility of high-quality cryoEM results. However, the cryoEM results are disappointing. The cryo 2D class averages and refined EM map in Fig S4 are of poor quality, indicating sub-optimal grid preparation or some other sample problem. Some of the FSC curves (2 in Fig S7 and 1 in Fig S6) have extremely peculiar shapes, suggesting something amiss in the map refinement. The sharp drop in the "corrected" FSC curves in Figs S5c and S6c (upper) indicate severe problems. The stated resolutions (3.42 & 3.82 Å) for the sNS1ts-Fab56.2 are wildly incompatible with the images of the refined maps in Figs 3 & S7. At those resolutions, clear secondary structural elements should be visible throughout the map. From the 2D averages and 3D maps shown in the figures this does not seem to be the case. Local resolution maps should be shown for each structure.*

The same sample is used for negative staining and the cryoEM results presented. The cryoEM 2D class averages are similar to the negative stain ones, with many spherical-like densities

with no discernible features, presumably HDL only or the NS1 features are averaged out. The key difference lies in the 2D class averages where the NS1 could be seen. The side views of NS1 (wing-like protrusion) are more obvious in the negative stain while the top views of NS1 (cross shaped-like protrusion) are more obvious under cryoEM. HDL particles are inherently heterogeneous and known to range from 70-120 Å, this has been highlighted in the main text (p. 8, lines 203 and 228). This helps to explain why the reviewer may find the cryoEM result disappointing. The sample is inherently challenging to resolve structurally as it is (not that the sample is of poor quality). In terms of grid preparation, Supp Fig 4b shows a representative motion-corrected micrograph of the isNS1ts sample whereby individual particles can be discerned and evenly distributed across the grid at high density.

We acknowledge that most of the dips in the FSC curves (Fig S5-7) are irregular and affect the accuracy of the stated resolutions, particularly for the HDL-isNS1ts-Fab56.2 and isNS1ts-Fab56.2 maps for which the local resolution maps are shown (Fig S7d-e). Probable reasons affecting the FSC curves include (1) the heterogeneous nature of HDL, (2) preferred orientation issue (p 7, lines 198 -200), and (3) the data quality is intrinsically less ideal for high resolution single particle analysis. Optimizing of the dynamic masking such that the mask is not sharper than the resolution of the map for the near (default = 3 angstroms) and far (12 angstroms) parameters during data processing, ranging from 6 - 12 and 14 - 20 respectively, did not help to improve the FSC curves. To report a more accurate global resolution, we have revised the figures S5-7 with new FSC curve plots generated using the remote 3DFSC processing server.

Regardless, the overall architecture and the relative arrangement of NS1 dimer, Fab, and HDL are clearly visible and identifiable in the map. These results agree well with our biochemical data and mass-spec data.

> *The samples were clearly challenging for cryoEM, leading to poor quality maps that were difficult to interpret. None of the figures are convincing that NS1, Ab56.2 or Fab56.2 are correctly fit into EM maps. There is no indication of ApoA1 helices. Details of the fit of models to density for key regions of the higher-resolution EM maps should be shown and the models should be deposited in the PDB. An example of modeling difficulty is clear in the sNS1ts dimer with bound Fab56.2 (figs 3c & S7e). For this complex, the orientation of the Fab56.2 relative to the sNS1ts dimer in this submission (Fig 3c) is substantially different than in the bioRxiv preprint (Fig 3c). Regions of empty density in Fig 3c also illustrate the challenge of building a model into this map.*

We acknowledge the modelling challenge posed by low resolution maps in general, such as the handedness of the Fab molecule as pointed out by the reviewer (which is why others have developed the use of anti-fab nanobody to aid in structure determination among other methods). The change in orientation of the Fab56.2 relative to the sNS1ts dimer was informed by the HDX-MS results which was not done at the point of bioRxiv preprint mentioned. With regards to indication of ApoA1 helices, this is expected given the heterogeneous nature of HDL. To the best of our knowledge, engineered apoA1 helices were also not reported in many cryoEM structures of membrane proteins solved in membrane scaffold protein (MSP) nanodiscs. This is despite nanodiscs, comprised of engineered apoA1 helices, having well-defined size classifications.

Regions of weak density in Fig 3c is expected due to the preferred orientation issue acknowledged in the results section of the main text (p. 9, line 245). The cryoEM density maps have been deposited in the Electron Microscopy Data Bank (EMDB) under accession codes EMD-36483 (isNS1ts:Fab56.2) and EMD-36480 (Fab56.2:isNS1ts:HDL). The protein model files for isNS1ts:Fab56.2 and Fab56.2:isNS1ts:HDL model are available upon request. Crosslinking MS raw files and the search results can be downloaded from https://repository.jpostdb.org/preview/14869768463bf85b347ac2 with the access code: 3827. The HDX-MS data is deposited

to the ProteomeXchange consortium via PRIDE partner repository51 with the dataset identifier PXD042235.

> *Mass spec:*
>
> *Crosslinking-mass spec was used to detect contacts between NS1 and ApoA1, providing strong validation of the sNS1-HDL association. As the crosslinks were detected in a bulk sample, they show that NS1 is near ApoA1 in many/most HDL particles, but they do not indicate a specific protein-protein complex. Thus, the data do not support the model of an NS1-ApoA1 complex in Fig 4d. Further, a specific NS1-ApoA1 interaction should have evidence in the EM maps (helical density for ApoA1), but none is shown or mentioned. If such exists, it could perhaps be visualized after focused refinement of the map for sNS1ts-HDL with Fab56.2 (Fig S7d). The finding that sNS1-ApoA1 crosslinks involved residues on the hydrophobic surface of the NS1 dimer confirms previous data that this NS1 surface engages with membranes and lipids.*

We thank the reviewer for the comment. The XL-MS is a method to identify the protein-protein interactions by proximity within the spacer arm length of the crosslinker. The crosslinking MS data do support the NS1-ApoA1 complex model obtained by cryo-EM because the identified crosslinks that are superimposed on the EM map are within the cut-off distance of 30 Å. We agree that the XL-MS data do not dictate the specific interactions between specific residues of NS1-ApoA1 in the EM model. We also do not claim that specific residue of NS1 in beta roll or wing domain is interacting with specific residue of ApoA1 in H4 and H5 domain. We claim that beta roll and wing domain regions of NS1 are interacting with ApoA1 in HDL indicating the proximity nature of NS1-ApoA1 interactions as warranted by the XL-MS data.

As explained in the previous response on the lack of indication of ApoA1 helical density, this is expected given the heterogeneous nature of HDL. It is typical to see lipid membranes as unstructured and of lower density than the structured protein. In our study, local refinement was performed on either the global map (presented in Fig S7d) or focused on the NS1-Fab region only. Both yielded similar maps as illustrated in the real space slices shown in Author response image 5. The mask and map overlay is depicted in similar orientations to the real space slices, and at different contour thresholds at 0.05 (Author response image 5e) and 0.135 (Author response image 5f). While the overall map is of poor resolution and directional anisotropy evident, there is clear signal differences in the low density region (i.e. the HDL sphere) indicative of NS1 interaction with ApoA1 in HDL, extending from the NS1 wing to the base of the HDL sphere.

Author response image 5.

Real Space Slices of map and mask used during Local Refinement for overall structure (a-b) and focused mask on NS1 region (c-d). The corresponding map (grey) contoured at 0.05 (e) and 0.135 (f) in similar orientations as shown for the real space slices of map and masks. The focused mask of NS1 used is colored in semi-transparent yellow. Real Space Slices of map and mask are generated during data processing in Cryosparc 4.0 and the map figures were prepared using ChimeraX.

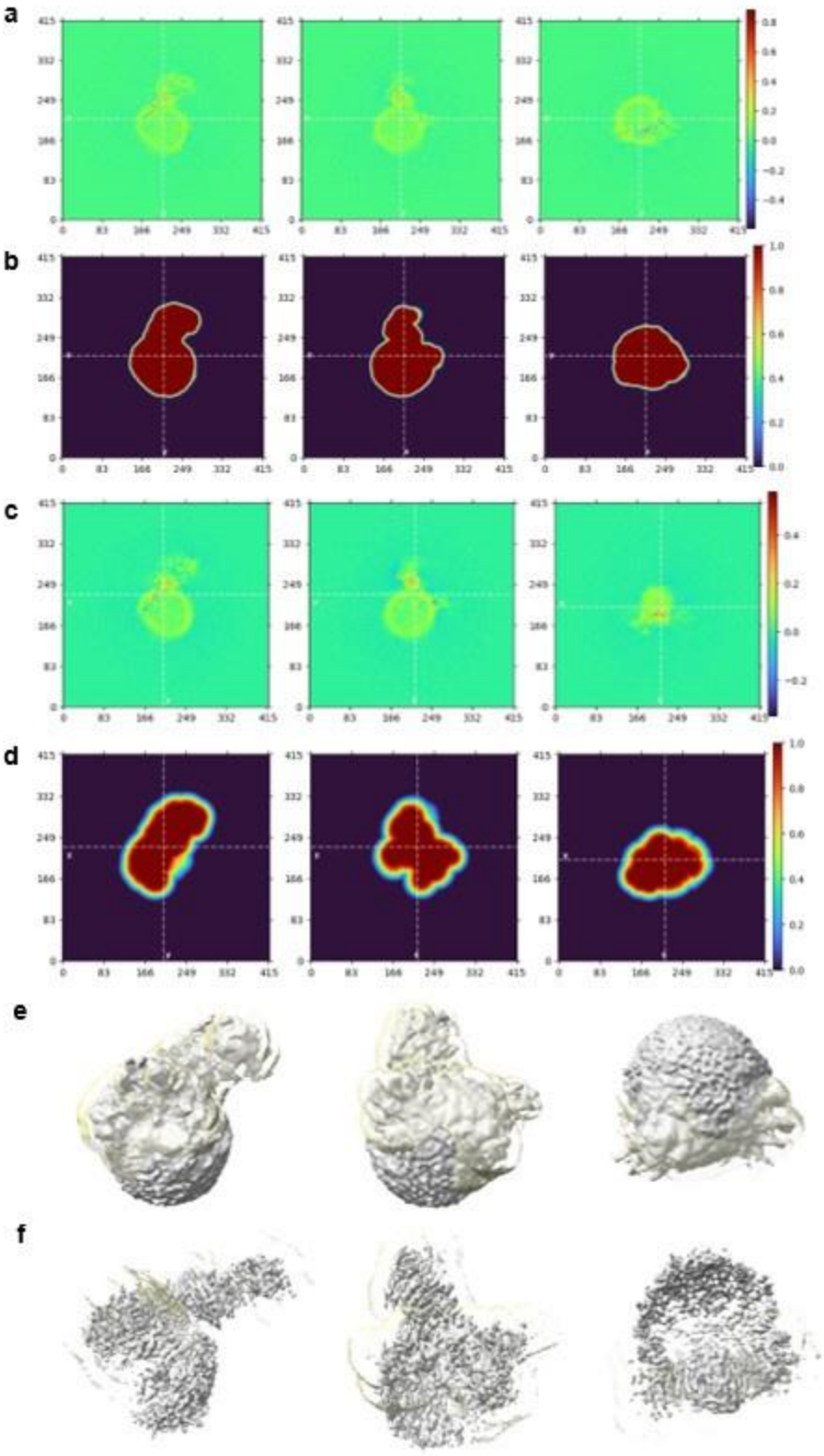

Sample quality:

The paper lacks any validation that the purified sNS1 retains established functions, for example the ability to enhance virus infectivity or to promote endothelial dysfunction.

Please see detailed response for question 2 in Reviewer #1's comments. In essence, we have showed that both isNS1wt and isNS1ts are capable of inducing endothelial permeability in an in vitro TEER assay (Rebuttal Fig 3) and also in our previous study that quantified inflammation in human PBMC's (Rebuttal Fig 2).

> *Peculiarities include the gel filtration profiles (Fig 2a), which indicate identical elution volumes (apparent MWs) for sNS1wt-HDL bound to Ab562 (~150 kDa) and to the ~3X smaller Fab56.2 (~50 kDa). There should also be some indication of sNS1wt-HDL pairs crosslinked by the full-length Ab, as can be seen in the raw cryoEM micrograph (Fig S5b).*
>
> *Obtaining high quality structures is often more demanding of sample integrity than are activity assays. Given the low quality of the cryoEM maps, it's possible that the acidification step in immunoaffinity purification damaged the HDL complex. No validation of HDL integrity, for example with acid-treated HDL, is reported.*

Please see detailed response for question 3 in Reviewer #1's comments.

> *Acid treatment is perhaps discounted by a statement (line 464) that another group also used immunoaffinity purification in a recent study (ref 20) reporting sNS1 bound to HDL. However the statement is incorrect; the cited study used affinity purification via a strep-tag on recombinant sNS1.*

We thank the Reviewer for pointing this out and have rewritten this paragraph instead (p 18, line 445-455). We also expanded our discussion to highlight our prior functional studies showing that acid-eluted isNS1 proteins do induce endothelial hyperpermeability (p 18-19, line 470-476).

> *Discussion:*
>
> *The Discussion reflects a view that the NS1 secreted from virus-infected cells is a 1:1 sNS1dimer:HDL complex with the specific NS1-ApoA1 contacts detected by crosslinking mass spec. This is inconsistent with both the neg-stain 2D class average with 2 sNS1 dimers on an HDL (Fig S1c) and with the recent study of Flamand & co-workers showing 1-3 NS1 dimers per HDL (ref 20). It is also ignores the propensity of NS1 to associate with membranes and lipids. It is far more likely that NS1 association with HDL is driven by these hydrophobic interactions than by specific protein-protein contacts. A lengthy Discussion section (lines 461-522) includes several chemically dubious or inconsistent statements, all based on the assumption that specific ApoA1 contacts are essential to NS1 association with HDL and that sNS1 oligomers higher than the dimer necessarily involve ApoA1 interaction, conclusions that are not established by the data in this paper.*

We thank the Reviewer and have revised our discussion to cover available structural and functional data to draw conclusions that invariably also need further validation by others. One point that is repeatedly brought up by Reviewer 1 & 2 is the quality and functionality of our sample. Our conclusion now reiterates this point based on our own published data (Chan et al., 2019) and also the TEER assay data provided as Author response image 3.

> ***Reviewer #1 (Recommendations For The Authors):***
>
> *Minor:*
>
> *(1) Fig. S3B, should the label for lane 4 be isNS1? In figure 1C you do not see ApoA1 for rsNS1 but for S3B you do? Which is correct?*

This has been corrected in the Fig. S3B, the label for lane 4 has been corrected to isNS1 and lane 1 to rsNS1, where no ApoA1 band (25 kDa) is found.

> *(2) Line 436, is this the correct reference? Reference 43?*

This has been corrected in the main text. (p 20, Line 507; Lee et al., 2020, J Exp Med).

> ***Reviewer #2 (Recommendations For The Authors):***
>
> *The cryoEM data analysis is incompletely described. The process (software, etc) leading to each refined EM map should be stated, including the use of reference structures in any step. These details are not in the Methods or in Figs S4-7, as claimed in the Methods. The use of DeepEMhancer (which refinements?) with the lack of defined secondary structural features in the maps and without any validation (or discussion of what was used as "ground truth") is concerning. At the least, the authors should show pre- and post-DeepEMhancer maps in the supplemental figures.*

The data processing steps in the Methods section have been described with improved clarity. DeepEMhancer is a deep learning solution for cryo-EM volume post-processing to reduce noise levels and obtain more detailed versions of the experimental maps (Sanchez-Garcia, et al., 2021). DeepEMhancer was only used to sharpen the maps and reduce the noise for classes 1 and 2 of isNS1wt in complex with Ab56.2 for visualization purpose only and not for any refinements. To avoid any confusion, the use of DeepEMhancer has been removed from the supp text and figures.

> *Line 83 - "cryoEM structures...recently reported" isn't ref 17*

This reference has been corrected in to Shu et al. (2022) in p 3, line 83.

> *Fig. S3 - mis-labeled gel lanes*

This has been corrected in the Fig. S3B, the label for lane 4 has been corrected to isNS1 and lane 1 to rsNS1.

> *Fig S6c caption - "Representative 2D classes of each 3D classes, white bar 100 Å. Refined 3D map for classes 1 and 2 coloured by local resolution". The first sentence is unclear, and there is no white scale bar and no heat map.*

Fig S6c caption has been corrected to “Representative 3D classes contoured at 0.06 and its particle distribution as labelled and coloured in cyan. Scale bar of 100 Å as shown. Refined 3D maps and their respective FSC resolution charts and posterior precision directional distribution as generated in crysosparc4.0”.